

Formation and Base Hydrolysis of Oxidimethaneamine Bridges in Co^{III} –Amine Complexes[†]

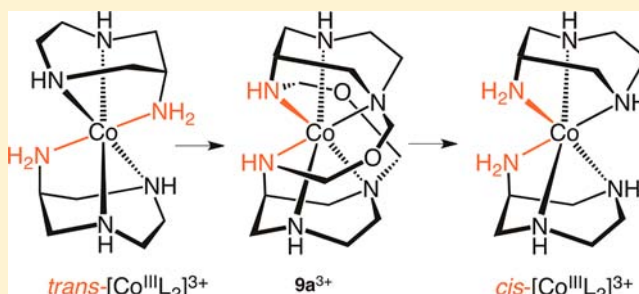
Bernd Morgenstern,[‡] Christian Neis,[‡] Anton Zschka,[‡] Jens Romba,[‡] Thomas Weyhermüller,[§] and Kaspar Hegetschweiler^{*‡}

[‡]Anorganische Chemie, Universität des Saarlandes, Postfach 15 11 50, D-66041 Saarbrücken, Germany

[§]MPI für Chemische Energiekonversion, Stiftstrasse 34-36, D-45470 Mülheim an der Ruhr, Germany

Supporting Information

ABSTRACT: *cis*-[CoL_2]³⁺ (**1a**³⁺), *trans*-[CoL_2]³⁺ (**2a**³⁺), *cis*-[$\text{Co}(\text{MeL})_2$]³⁺ (**1b**³⁺), and *trans*-[$\text{Co}(\text{MeL})_2$]³⁺ (**2b**³⁺), L = 1,4-diazepan-6-amine (daza) and MeL = 6-methyl-1,4-diazepan-6-amine (Medaza), were allowed to react as templates in acetonitrile with paraformaldehyde and triethylamine. Several Co^{III} complexes, where two adjacent amino groups of two ligand moieties are interlinked by an oxidimethaneamine bridge, were obtained. Connection of a primary with a secondary amino group (prim–sec bridging) was found to be predominant. The singly and doubly bridged daza- and Medaza-derivatives **7a**³⁺, **9a**³⁺ and **7b**³⁺, **9b**³⁺ were characterized by crystal-structure analysis. The bridging process resulted in a slight lengthening of the mean Co–N distance, a red shift of the A_{1g} – T_{1g} transition, and an increase of the $\text{Co}^{\text{III}}/\text{Co}^{\text{II}}$ reduction potential. Several minor components, which could be only partially separated by chromatographic methods, were also formed. The daza-derivatives **6a**³⁺ (prim–prim bridged) and **10a**³⁺ (bidentate coordination of one daza frame) formed in small quantities. The Medaza derivatives **3b**³⁺ and **4b**³⁺ (trans configuration of the Medaza frames, with additional pending carbinolamino groups), and **8b**³⁺ (with a methylideneimino group) represent intermediates of the condensation process. Their structure was again corroborated by X-ray diffraction. All bridged species (**6a**³⁺, **7a**³⁺, **7b**³⁺, **8b**³⁺, **9a**³⁺, **9b**³⁺, and **10a**³⁺) exhibited exclusively a *cis* orientation of the two diazepane frames, even if the *trans* configured **2a**³⁺ or **2b**³⁺ were used as starting materials. Molecular mechanics calculations indicate that in the bridged species with a *trans* configuration steric strain is substantially more pronounced. In alkaline aqueous media, **9a**³⁺ and **9b**³⁺ revealed a complete degradation of the bridges whereby the original **1a**³⁺ and **1b**³⁺ reformed. The pseudo-first-order rate constant k^{obs} of the degradation reaction was found to depend linearly on OH^- concentration. The degradation of the first bridge is about 100 times faster than the degradation of the second. The mechanism of formation and degradation of such oxidimethaneamine bridges is discussed.



INTRODUCTION

Co^{III} -polyamine complexes have frequently been used as templates for the synthesis of polyaza macrocycles.¹ It has been established that in an alkaline medium the coordinated amino group readily reacts with formaldehyde, yielding a corresponding carbinolamine (Scheme 1). Both the primary and secondary amino groups may undergo this type of reaction, but only the primary amino group is available for a subsequent H_2O elimination, forming a corresponding methylideneimine. Coordinated methylideneimines display a distinct reactivity as electrophiles. As such, they represent valuable synthons, reacting with various types of nucleophiles.² It is, however, noteworthy that coordinated methylideneimines are surprisingly unreactive against water as long as the pH is maintained below 7. Some of them have even been isolated in the solid state from an acidic aqueous medium.^{3,4}

[†]Facially Coordinating Cyclic Triamines, 6. – Part 5: Ref 8.

The alcoholic oxygen donor of a coordinated carbinolamine reacts as a nucleophile, and the reaction with an adjacent methylideneimine results in the formation of an oxidimethaneamine bridge (Scheme 1).^{4–6} This type of reaction is thus straightforward for the bridging of a primary and a secondary amino group, but is not possible for two secondary amino groups. The bridging of two primary amino groups is also possible⁴ but will only occur if the attack of the imine by an adjacent carbinolamine is faster than H_2O elimination of the latter.

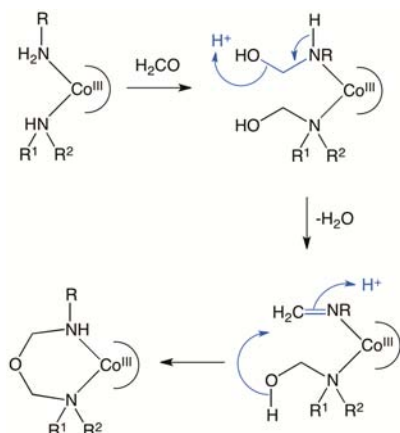
With this focus, polyamine ligands containing both primary and secondary amino groups are of particular interest. In a previous report,⁴ we investigated *cis*- and *trans*-[$\text{Co}(\text{dapi})_2$]³⁺ (dapi = *cis*-3,5-diamino-piperidine) as templates and characterized condensation products with one or two oxidimethaneamine bridges, respectively. It has been found that the coordinated oxidimethaneamine bridges are of high stability.

Received: July 23, 2013

Published: October 2, 2013

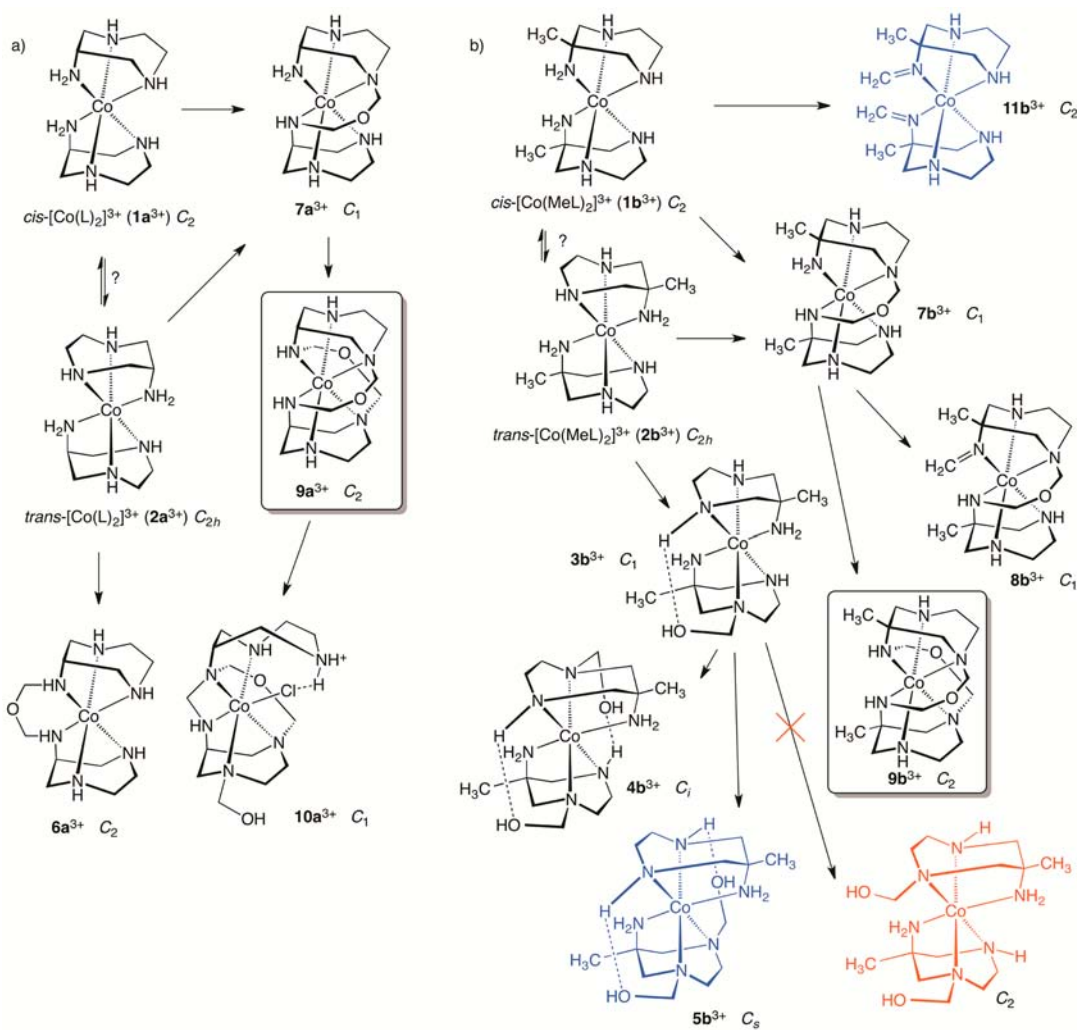


Scheme 1. Schematic Representation of the Reactivity of Primary and Secondary Amines Coordinated to Co^{III} with Formaldehyde in an Alkaline, Nonaqueous Medium



However, it is also known that these species decompose in an alkaline medium.^{5,6} In the investigation reported here, new oxidimethaneamine-bridged Co^{III} complexes with 1,4-diazepan-6-amine (daza = L)⁷ and 6-methyl-1,4-diazepan-6-amine (Medaza = MeL)^{8,9} have been prepared. These two ligands are of interest because they represent a complement to dapi, with the number of primary and secondary amino groups being inverted. In the first part, *cis*- $[\text{CoL}_2]^{3+}$ (**1a**³⁺), *cis*- $[\text{Co}(\text{MeL})_2]^{3+}$ (**1b**³⁺), *trans*- $[\text{CoL}_2]^{3+}$ (**2a**³⁺), and *trans*- $[\text{Co}(\text{MeL})_2]^{3+}$ (**2b**³⁺) were subjected to reaction with paraformaldehyde in an alkaline, nonaqueous medium.¹⁰ We thoroughly studied the condensation process under variable conditions, and we were able to characterize some intermediates that previously have been proposed but have not been isolated yet (Scheme 2). In the second part, we performed a kinetic study of the base-catalyzed degradation of the oxidimethaneamine bridge in aqueous solution. We located characteristic differences in the reaction rate for different species, and we will demonstrate that such differences can be used to isolate derivatives that are difficult to obtain by a direct formation process. As far as we are aware, this is

Scheme 2. Synopsis for the Reactivity of $[\text{Co}^{\text{III}}(\text{daza})_2]^{3+}$ (a) and $[\text{Co}^{\text{III}}(\text{Medaza})_2]^{3+}$ (b) with Paraformaldehyde in MeCN and Triethylamine^a



^aThe species that were characterized by single-crystal X-ray structure analysis are shown in black. The species that have been identified in solution by NMR spectroscopy are drawn in blue, and the red structure refers to a nonobserved species. The two main products with two prim-sec-oxidimethaneamine bridges are boxed.

Table 1. Kinetic Data and Experimental Conditions of Bridge Degradation in Alkaline Aqueous Solution Obtained by CV or NMR Measurements as Indicated

pH ^a	type of reaction	k^{obs} (s ⁻¹) ^b	R^c	N^d	buffer ^e
CV ^f					
6.40	9a ³⁺ → 7a ³⁺	1.8(1) × 10 ⁻⁵	0.9679	7	Bis-Tris
	9b ³⁺ → 7b ³⁺	2.6(1) × 10 ⁻⁵	0.9895	8	Bis-Tris
7.10	9a ³⁺ → 7a ³⁺	1.1(1) × 10 ⁻⁴	0.9780	9	Imidazole
	9b ³⁺ → 7b ³⁺	1.53(3) × 10 ⁻⁴	0.9979	7	Imidazole
7.52	9a ³⁺ → 7a ³⁺	2.55(2) × 10 ⁻⁴	0.9993	17	HEPPS
	7a ³⁺ → 1a ³⁺	3.16(2) × 10 ⁻⁶	0.9997	8	HEPPS
	9b ³⁺ → 7b ³⁺	3.9(1) × 10 ⁻⁴	0.9962	9	HEPPS
	7b ³⁺ → 1b ³⁺	3.1(1) × 10 ⁻⁶	0.9928	6	HEPPS
8.00	9a ³⁺ → 7a ³⁺	7.18(3) × 10 ⁻⁴	0.9997	17	HEPPS
	7a ³⁺ → 1a ³⁺	9.5(6) × 10 ⁻⁶	0.9643	10	HEPPS
	9b ³⁺ → 7b ³⁺	1.23(2) × 10 ⁻³	0.9975	10	HEPPS
8.50	9a ³⁺ → 7a ³⁺	2.35(3) × 10 ⁻³	0.9989	7	HEPPS
	7a ³⁺ → 1a ³⁺	4.5(1) × 10 ⁻⁵	0.9972	5	HEPPS
	9b ³⁺ → 7b ³⁺	3.25(4) × 10 ⁻³	0.9986	10	HEPPS
	7b ³⁺ → 1b ³⁺	3.17(4) × 10 ⁻⁵	0.9988	10	HEPPS
9.00	9a ³⁺ → 7a ³⁺	[4.5(2) × 10 ⁻³]	0.9909	9	CHES
	7a ³⁺ → 1a ³⁺	1.04(2) × 10 ⁻⁴	0.9986	5	CHES
9.50	9a ³⁺ → 7a ³⁺	[1.38(1) × 10 ⁻²]	0.9995	8	CHES
	7a ³⁺ → 1a ³⁺	1.62(5) × 10 ⁻⁴	0.9891	12	CHES
	9b ³⁺ → 7b ³⁺	[2.8(7) × 10 ⁻²]	0.8825	3	CHES
	7b ³⁺ → 1b ³⁺	2.13(3) × 10 ⁻⁴	0.9983	10	CHES
10.00	7a ³⁺ → 1a ³⁺	7.4(2) × 10 ⁻⁴	0.9949	8	CAPS
10.50	7a ³⁺ → 1a ³⁺	3.2(1) × 10 ⁻³	0.9911	9	CAPS
	7b ³⁺ → 1b ³⁺	2.63(6) × 10 ⁻³	0.9944	12	CAPS
11.00	7a ³⁺ → 1a ³⁺	[4.57(6) × 10 ⁻³]	0.9990	7	CAPS
11.60	7a ³⁺ → 1a ³⁺	[1.61(4) × 10 ⁻²]	0.9972	6	CAPS
NMR ^f					
6.80	9b ³⁺ → 7b ³⁺	2.36(6) × 10 ⁻⁵	0.9922	14	Imidazole
7.69	9b ³⁺ → 7b ³⁺	2.10(3) × 10 ⁻⁴	0.9969	14	HEPPS
	7b ³⁺ → 1b ³⁺	2.1(2) × 10 ⁻⁶	0.9565	7	HEPPS
8.41	9b ³⁺ → 7b ³⁺	1.26(3) × 10 ⁻³	0.9908	16	HEPPS
	7b ³⁺ → 1b ³⁺	9.5(3) × 10 ⁻⁶	0.9957	6	HEPPS
8.90	9b ³⁺ → 7b ³⁺	3.9(1) × 10 ⁻³	0.9976	6	Taurine
	7b ³⁺ → 1b ³⁺	3.50(5) × 10 ⁻⁵	0.9967	20	Taurine
10.20	7b ³⁺ → 1b ³⁺	5.39(9) × 10 ⁻⁴	0.9954	18	Taurine
10.60	7b ³⁺ → 1b ³⁺	9.0(1) × 10 ⁻⁴	0.9972	15	Na ₂ CO ₃
11.00	7b ³⁺ → 1b ³⁺	2.13(4) × 10 ⁻³	0.9952	12	Na ₂ CO ₃

^aFor pH measurement in D₂O, see ref 12. ^bStandard deviations are given in parentheses. The values in square brackets refer to conditions where the reaction was too fast for a reliable determination. ^cCorrelation coefficient for the linear regression analysis of ln [A]/[A]₀ vs time. ^dNumber of data points. ^eThe total buffer concentration was 0.1 M. Bis-Tris, bis(2-hydroxyethyl)amino-tris(hydroxymethyl)methane; HEPPS, 3-[4-(2-hydroxyethyl)piperazin-1-yl]propane-1-sulfonic acid; CHES, 2-(cyclohexylamino)ethanesulfonic acid; CAPS, 3-(cyclohexylamino)-1-propane-sulfonic acid; imidazole, 1,3-diazole; taurine, 2-aminoethanesulfonic acid. ^fThe reactions were carried out at 25 °C in H₂O (CV) or at 21 °C in D₂O (NMR) in 2 M KCl.

the first Article that reports explicitly the kinetic data of such degradation reactions.

EXPERIMENTAL SECTION

Materials and Instrumentation. Commercially available chemicals were of reagent grade and were used as obtained. For the synthetic procedures in the absence of water, absolute solvents were purchased. SP-Sephadex C-25 and Dowex 50 W-X2 (100–200 mesh, H⁺ form) were from Sigma-Aldrich. The presence of Co²⁺ in the various fractions of the chromatographic procedure was verified using Merckoquant test strips. The trichloride salts of 1³⁺ and 2³⁺ were prepared as described previously;^{7,8} however, careful drying in vacuo yielded products with a lower content of water of crystallization. For 1aCl₃·H₂O, Anal. Calcd (%) for C₁₀H₂₈Cl₃CoN₆O (413.66): C, 29.04; H, 6.82; N, 20.32. Found: C, 29.22; H, 6.57; N, 20.10. For 1bCl₃·1.5H₂O, Anal. Calcd (%) for C₁₂H₃₃Cl₃CoN₆O_{1.5} (450.72): C, 31.98; H, 7.38; N, 18.65. Found: C,

32.27; H, 7.05; N, 18.53. For 2aCl₃·2H₂O, Anal. Calcd (%) for C₁₀H₃₀Cl₃CoN₆O₂ (431.68): C, 27.82; H, 7.01; N, 19.47. Found: C, 27.66; H, 6.73; N, 19.03. For 2bCl₃·2H₂O, Anal. Calcd (%) for C₁₂H₃₄Cl₃CoN₆O₂ (459.73): C, 31.35; H, 7.45; N, 18.28. Found: C, 31.65; H, 7.06; N, 18.38. Solutions of the trifluoromethanesulfonate salts of 7³⁺ and 9³⁺ (for UV–vis spectroscopy in CH₃CN/NEt₃) were prepared by suspending the trichlorides in CH₃CN. Three equiv of AgCF₃SO₃ was then added. The mixture was stirred for 5 min, and the precipitated AgCl was filtered off.

UV–vis spectra of 3b³⁺ (1 M aq HCl), 8b³⁺ (1 M aq HCl), the deprotonation products of 7³⁺ and 9³⁺ (CH₃CN),¹⁰ and the dark colored product solutions obtained from the bridging reaction (CH₃CN, Figure S1) were recorded on a Varian Cary 50 spectrophotometer; all other samples (1 M aq HCl) were measured on a Uvikon 941 spectrophotometer. IR spectra were recorded on a Bruker Vector 22 FT IR spectrometer equipped with a Golden Gate

Table 2. Product Distribution for the Reaction of 1³⁺ and 2³⁺ with Paraformaldehyde and Triethylamine in Acetonitrile

Starting material ^a	<i>cis</i> -[CoL ₂] ³⁺ 1a ³⁺	<i>trans</i> -[CoL ₂] ³⁺ 2a ³⁺	<i>cis</i> -[CoL ₂] ³⁺ 1a ³⁺	<i>cis</i> -[Co(MeL) ₂] ³⁺ 1b ³⁺	<i>trans</i> -[Co(MeL) ₂] ³⁺ 2b ³⁺
Method ^b	(i)	(i)	(ii)	(ii)	(iii)
H ₂ O content ^c	< 2	< 2	36	27	< 2
Rate	slow ^d	slow ^d	fast ^e	fast ^e	slow ^d
Fraction No.					
1	yellowish-orange H ₃ L ³⁺ ; 7a ³⁺ (< 5 %) ^f	yellow H ₃ L ³⁺ ; 6a ^{3+g}	pink H ₃ MeL ³⁺ ; ≥ 2 unknown non-imine species Altogether: < 2 % ^f	yellowish-orange 3b ³⁺ (9 %) ^f	
2	orange 9a ³⁺ (75 %) ^f	yellowish-orange H ₃ L ³⁺ ; 7a ³⁺ (< 10 %) ^f	yellow, H ₃ MeL ³⁺ ; 11b ^{3+,i} ; ≥ 2 unknown non-imine species; 7b ³⁺ Altogether: < 5 % ^f	orange 9b ³⁺ (41 %) ^f	
3		orange purple tail 9a ³⁺ (85 %) ^f ; 10a ^{3+g}	orange 9b ³⁺ (65 %) ^f	light-orange 4b ³⁺ (15 %) ^{f,h} ; 5b ³⁺ (10 %) ^{f,h}	
4			yellow 8b ³⁺ ; 2 unknown non-imine species Altogether: < 5 % ^f		

^aSupplied as trifluoromethanesulfonate salts. L, daza; MeL, Medaza. ^bRoom temperature, addition of water as indicated, analysis of the main fractions was obtained after chromatography on a 2 m Sephadex column. See the Experimental Section for details. ^cEquival of H₂O per equiv of complex in the reaction mixture. ^dAfter the combination of the ingredients, a color change to slight gray was noted. The mixture darkened steadily until a deep black slurry was obtained after 30 min. ^eAfter the combination of the ingredients, the color turned to deep black within a few seconds. ^fThe yields stated refer to the total amount of Co. The reproducibility is ±5% unless otherwise stated. ^gSmall amount with poor reproducibility (was not always observed). ^hTogether with some minor unidentified byproducts. ⁱThe imine- and methyl-region in the NMR spectrum of this species is compatible with a C₂-symmetric bis-imine complex, see ref 27.

ATR unit. The ¹H NMR spectrum of a mixture of **4b** and **5b** was recorded on a Bruker Avance 700 spectrometer (resonance frequency: 700.45 MHz); all other ¹H and ¹³C{¹H} NMR spectra were measured on a Bruker DRX Avance 400 MHz NMR spectrometer (resonance frequencies: 400.13 MHz for ¹H and 100.6 MHz for ¹³C). The temperature was 21 °C unless otherwise specified. D₂O was used as the solvent throughout. Chemical shifts are given in ppm relative to D₄-sodium (trimethylsilyl)propionate as the internal standard (δ = 0 ppm). Two-dimensional spectra were measured as gradient-selected ¹H–¹³C HMBG or HMQC and ¹H–¹H COSY experiments.¹¹ Unless otherwise specified, the spectra of the oxidimethaneamine-bridged species were measured in 0.1 M DCl to avoid decomposition. For the kinetic study (bridge cleavage of **9b**³⁺ and **7b**³⁺), appropriate buffers (0.1 M total concentration, Table 1) were dissolved in D₂O. KCl was added to guarantee an ionic strength of 2 M, and the pH¹² was adjusted with D₂O solutions of DCl or NaOD. About 5 mg of solid **9b**Cl₃·4H₂O was added, and the solution was immediately transferred into the spectrometer. For each data point, a total of eight scans with a sweep width of 2 ppm were recorded, requiring a measuring time of about 30 s.

Cyclic Voltammetry. All cyclic voltammograms were recorded at 25 ± 2 °C using a Metrohm 797 VA Computrace potentiostat, a hanging mercury drop working electrode (HMDE), a Pt counter electrode, and a Ag/AgCl reference electrode with a certified potential of 208.7 mV versus SHE (checked against [Fe(phen)₂](ClO₄)₂ in 1.0 M H₂SO₄, E_{1/2} = 106 mV).¹³ All potentials given in this Article refer to the SHE. For the kinetic study (bridge cleavage of **9**³⁺ and **7**³⁺), KCl and an appropriate buffer (Table 1) were dissolved in water, and the pH was adjusted with HCl or KOH. Nineteen milliliters of this solution was placed in the measuring cell, and the reaction was started by the addition of the complex, which had been predissolved in 1 mL of water. The final concentrations were 2 M KCl, 0.1 M buffer, and 5 mM total Co. For each data point, three scans were recorded with a sweep rate of 0.3 V s⁻¹ and a

scan range of –0.9 to –0.1 V, requiring a total measuring time of about 30 s.

Molecular Mechanics Calculations. Molecular mechanics calculations were carried out as described previously^{8,14} using the program HyperChem¹⁵ for visualization and the program MOMECC97¹⁶ with an extended force field¹⁷ for structure optimization and energy minimization. It has been shown that the MOMECC force field reproduces the structures of low-spin Co^{III}-amine complexes reliably and calculates meaningful differences for the strain energy of diastereomeric complexes.^{18,19} All energy minimization calculations converged (<0.001 Å) without problems, and the calculated structures generally exhibited meaningful bond distances and angles.

Synthetic Work. **1b**[ZnCl₄]Cl·2H₂O. **1b**Cl₃·1.5H₂O (35 mg, 0.08 mmol) was dissolved in water (5 mL). ZnCl₂, dissolved in 3 M HCl (5 mL), was added. The solution was allowed to evaporate slowly under ambient conditions. Orange needles suitable for X-ray structure analysis appeared after 1 day. The crystals, which tend to effloresce slowly, were dried in vacuo. Anal. Calcd (%) for C₁₂H₃₄Cl₅CoN₆O₂Zn (596.02): C, 24.18; H, 5.75; N, 14.10. Found: C, 24.20; H, 5.75; N, 14.26. IR (cm⁻¹): 597, 605, 639, 654, 704, 790, 831, 929, 981, 1006, 1034, 1065, 1134, 1169, 1225, 1305, 1361, 1382, 1425, 1453, 1549, 1586, 2333, 2362, 3074, 3191.

2b[ZnCl₄]Cl·H₂O. **2b**Cl₃·2H₂O (50 mg, 0.11 mmol) was converted into the [ZnCl₄]Cl salt as described above for **1b**³⁺. Orange needles suitable for X-ray structure analysis appeared after 3 days. They were dried in vacuo. Anal. Calcd (%) for C₁₂H₃₂Cl₅CoN₆O₂Zn (578.00): C, 24.94; H, 5.58; N, 14.54. Found: C, 24.42; H, 5.23; N, 14.08. IR (cm⁻¹): 614, 626, 654, 719, 794, 813, 830, 908, 930, 975, 1005, 1056, 1136, 1168, 1214, 1258, 1305, 1363, 1422, 1485, 1580, 3116 (br), 3436, 3516.

1a(CF₃SO₂)₃. CF₃SO₂H (10 mL) was added to **1a**Cl₃·H₂O (1.5 g, 3.6 mmol). The resulting viscous solution was heated at 80 °C, and a stream of N₂ was passed through the solution for 4 h. After cooling to room

temperature, the orange solution was poured into Et₂O (500 mL). A yellow solid precipitated immediately, which was collected on a Büchner funnel, washed several times with Et₂O, and dried in vacuo.^{20,21} Yield: 2.6 g (3.1 mmol, 86%) of a yellowish orange solid of composition **1a** (CF₃SO₃)₃·0.7CF₃SO₃H. Anal. Calcd (%) for C_{13.7}H_{26.7}CoF_{11.1}N₆O_{11.1}S_{3.7} (841.55): C, 19.55; H, 3.20; N, 9.99. Found: C, 19.53; H, 3.41; N, 9.93. IR (cm⁻¹): 513, 523, 546, 554, 572, 589, 625, 762, 823, 850, 886, 941, 985, 1021, 1047, 1087, 1144, 1111, 1160, 1222, 1500, 1613, 3235. ¹H NMR δ 2.70 (d, *J* = 13 Hz, 4H), 3.03 (m, 4H), 3.40–3.53 (m, 8H), 3.73 (m, 2H), 5.16 (br, NH), 5.26 (br, NH), 6.36 (br, NH), 6.87 (br, NH). ¹³C {¹H} NMR δ 55.9, 56.6, 57.7, 57.8, 62.2, 122.6 (q, *J* = 317 Hz). A small quantity was washed again with Et₂O to remove the inherent trifluoromethanesulfonic acid. Anal. Calcd (%) for C₁₃H₂₆CoF₉N₆O₉S₃ (736.49): C, 21.20; H, 3.56; N, 11.41. Found: C, 21.50; H, 3.30; N, 11.02.

2a(CF₃SO₃)₃. The method described above for the *cis* isomer was applied. **2a**Cl₃·2H₂O (1.5 g, 3.5 mmol) yielded 2.6 g (3.5 mmol, 100%) of a yellowish orange solid. Anal. Calcd (%) for C₁₃H₂₆CoF₉N₆O₉S₃ (736.49): C, 21.20; H, 3.56; N, 11.41. Found: C, 21.07; H, 3.47; N, 11.12. IR (cm⁻¹): 523, 540, 559, 574, 586, 631, 760, 984, 1022, 1046, 1161, 1184, 1220, 1239, 1252, 1498, 1604, 3159, 3242. ¹H NMR δ 2.68 (d, *J* = 14 Hz, 4H), 2.88 (m, 4H), 3.37 (m, 4H), 3.40 (br, 2H), 3.55 (d, *J* = 14 Hz, 4H). ¹³C {¹H} NMR δ 55.7, 56.9, 62.4, 122.6 (q, *J* = 317 Hz).

1b(CF₃SO₃)₃·2H₂O. The method described above for **1a**³⁺ was applied. **1b**Cl₃·1.5H₂O (1.1 g, 2.4 mmol) yielded 1.8 g (2.2 mmol, 92%) of a yellowish orange solid. Anal. Calcd (%) for C₁₅H₃₄CoF₉N₆O₁₁S₃ (800.58): C, 22.50; H, 4.28; N, 10.50. Found: C, 22.52; H, 3.86; N, 10.21. IR (cm⁻¹): 504, 516, 551, 568, 628, 760, 829, 853, 930, 980, 1023, 1065, 1161, 1222, 1446, 1464, 1483, 1498, 1600, 3134, 3213. ¹H NMR δ 1.37 (s, 6H), 2.69 (d, *J* = 7 Hz, 2H), 2.72 (d, *J* = 7 Hz, 2H), 3.05 (m, 4H), 3.37–3.45 (m, 6H), 3.70 (m, 2H). ¹³C {¹H} NMR δ 20.4, 55.8, 56.4, 64.7, 66.6, 66.8, 122.6 (q, *J* = 317 Hz).

2b(CF₃SO₃)₃·0.5CF₃SO₃H·0.75H₂O. The method described above for **1a**³⁺ was applied. Despite extensive washing with Et₂O, a complete removal of trifluoromethanesulfonic acid was not possible. **2b**Cl₃·2H₂O (2.3 g, 5.0 mmol) yielded 4.2 g (4.9 mmol, 98%) of a yellowish-orange solid. Anal. Calcd (%) for C_{15.5}H₃₂CoF_{10.5}N₆O_{11.25}S_{3.5} (853.10): C, 21.82; H, 3.78; N, 9.85. Found: C, 21.58; H, 3.76; N, 9.53. IR (cm⁻¹): 505, 516, 533, 559, 574, 629, 763, 814, 833, 914, 938, 977, 1021, 1061, 1156, 1219, 1239, 1370, 1386, 1434, 1464, 1499, 1600, 1633, 3145, 3237. ¹H NMR δ 1.33 (s, 6H), 2.68 (d, *J* = 14 Hz, 4H), 2.88 (m, 4H), 3.39–3.47 (m, 8H), 5.12 (br, NH), 6.94 (br, NH). ¹³C {¹H} NMR δ 20.1, 55.9, 64.3, 67.2, 122.6 (q, *J* = 317 Hz).

Bridging Reaction (the Numbering of the Methods Refers to Table 2). *Method (i).* **1a**(CF₃SO₃)₃·0.7CF₃SO₃H (2.5 g, 3.0 mmol) or **2a**(CF₃SO₃)₃ (2.6 g, 3.5 mmol) was dissolved in acetonitrile (100 mL). NEt₃ (28.4 mL, 0.20 mol) was added. A clear orange solution was obtained. After the addition of paraformaldehyde (12.28 g, 0.41 mol), an opaque black mixture was formed within a period of 30 min.

Method (ii). **1a**(CF₃SO₃)₃·0.7CF₃SO₃H (1.2 g, 1.4 mmol) or **1b**(CF₃SO₃)₃·2H₂O (1.1 g, 1.4 mmol) was dissolved in acetonitrile (100 mL). An orange solution was obtained. H₂O (900 μL), triethylamine (9.95 mL, 0.07 mol), and paraformaldehyde (5.89 g, 0.20 mol) were added in this order. After paraformaldehyde addition, an abrupt color change to opaque black was observed.

Method (iii). **2b**(CF₃SO₃)₃·0.5(CF₃SO₃H)·0.75H₂O (1.9 g, 2.2 mmol) and paraformaldehyde (9.04 g, 0.30 mol) were placed in a 250 mL flask. Triethylamine (20.89 mL, 0.15 mol) was added. In the last step, acetonitrile (100 mL) was added. The color changed slowly to black, and after 30 min an opaque black suspension was finally observed.

Work Up. The reaction mixtures were poured into 1 M H₂SO₄. The color changed instantaneously to orange. Excess solid paraformaldehyde was filtered off and washed with water. The combined filtrates were diluted with distilled water to a total volume of 400 mL and sorbed on Dowex 50. The columns were washed with H₂O (1 L), 0.5 M HCl (1 L), and 1 M HCl (1 L). The products were eluted with aqueous 3 M HCl (1.5 L). The resulting colored fractions were evaporated to dryness under reduced pressure, yielding orange solids that were dissolved in a small amount of 0.2 M Na₂SO₄ (10 mL, where pH 4 was adjusted with a few drops of H₂SO₄). The solutions were sorbed on Sephadex (2 m

column length, 3 cm diameter) and eluted with 0.2 M Na₂SO₄ (pH 4). Several bands evolved (Table 2), which were collected separately, desalted on Dowex 50 (3 M HCl), and evaporated to dryness. In the case of method (ii) with **1a**³⁺ as the starting material, fraction 3 sometimes exhibited a small amount of a purple tail, which did not separate completely from the bulk orange portion. However, a separate collection of the head and the last part of the tail allowed the isolation of a mixture from which pure **10a**³⁺ could be crystallized.

Characterization. **3b**Cl₃·3.5H₂O. Anal. Calcd (%) for C₁₃H₃₉Cl₃CoN₆O_{4.5} (516.78): C, 30.21; H, 7.61; N, 16.26. Found: C, 30.18; H, 7.31; N, 15.61. ¹H NMR δ 1.38 (s, 3H), 1.40 (s, 3H), 2.62–2.99 (m, 8H), 3.33 (d, *J* = 14 Hz, 1H), 3.37–3.74 (m, 7H), 4.42 (d, *J* = 9 Hz, 1H), 4.51 (d, *J* = 9 Hz, 1H), 4.99 (br, d, *J* = 9 Hz, 1H), 5.21 (br, d, *J* = 9 Hz, 1H), 5.33 (br, d, *J* = 9 Hz, 1H), 5.72 (br, d, *J* = 9 Hz, 1H), 6.83 (br, t, 1H), 6.97 (br, t, 1H), 7.03 (br, t, 1H). ¹³C {¹H} NMR δ 20.2, 20.4, 55.4, 55.7, 56.0, 59.2, 64.3, 64.5, 67.3, 67.5, 67.6, 69.4, 85.5. UV–vis λ_{max} [nm] (ε[M⁻¹ cm⁻¹]): 478 (92), 341 (97).

Single crystals of 3b(ClO₄)₃. **3b**Cl₃·3.5H₂O was dissolved in 3 M HClO₄. The solution was allowed to evaporate slowly under ambient conditions. Orange crystals, suitable for X-ray structure analysis, were obtained after a few days. IR (cm⁻¹): 499, 518, 553, 575, 619, 679, 710, 788, 813, 829, 922, 967, 1037, 1178, 1221, 1324, 1368, 1382, 1394, 1422, 1468, 1491, 1504, 1603, 3159, 3234, 3265, 3375.

*Mixture of 4b and 5b*Cl₃·2.5H₂O. Anal. Calcd (%) for C₁₄H₃₉Cl₃CoN₆O_{4.5} (528.79): C, 31.80; H, 7.43; N, 15.89. Found: C, 31.93; H, 7.03; N, 15.06. ¹H NMR (700 MHz) indicated a ratio **4b**³⁺/**5b**³⁺ of 3:2. For **4b**³⁺, ¹H NMR δ 1.43 (s, 6H), 2.67 (d, *J* = 13 Hz, 2H), 2.67 (m, 2H), 2.74 (d, *J* = 13 Hz, 2H), 2.93 (m, 2H), 3.32 (d, *J* = 14 Hz, 2H), 3.50 (m, 2H), 3.58 (m, 2H), 3.71 (d, *J* = 13 Hz, 2H), 4.30 (d, *J* = 9 Hz, 2H), 4.34 (d, *J* = 9 Hz, 2H). For **5b**³⁺, ¹H NMR δ 1.41 (s, 3H), 1.44 (s, 3H), 2.62 (d, *J* = 13 Hz, 2H), 2.78 (m, 2H), 2.79 (m, 2H), 2.84 (m, 2H), 3.44 (d, *J* = 13 Hz, 2H), 3.47 (d, *J* = 8 Hz, 2H), 3.59 (m, 2H), 3.61 (m, 2H), 4.43 (d, *J* = 9 Hz, 2H), 4.45 (d, *J* = 9 Hz, 2H). ¹³C {¹H} NMR **4b**³⁺: δ 20.4, 55.1, 59.5, 64.1, 67.7, 69.8, 85.5. ¹³C {¹H} NMR **5b**³⁺: δ 20.3, 20.5, 55.8, 58.7, 63.6, 64.4, 67.6, 69.9, 85.7.

Single Crystals of 4bCl₃·3H₂O. The mixture of [**4b** and **5b**]Cl₃·2.5 H₂O was dissolved in 3 M HCl. Slow evaporation under ambient conditions yielded orange crystals suitable for X-ray structure analysis. Anal. Calcd (%) for C₁₄H₄₀Cl₃CoN₆O₅ (537.80): C, 31.27; H, 7.50; N, 15.63. Found: C, 31.62; H, 7.36; N, 15.21. IR (cm⁻¹): 505, 521, 533, 541, 559, 576, 664, 838, 875, 920, 950, 998, 1027, 1057, 1121, 1144, 1178, 1247, 1312, 1371, 1422, 1485, 1504, 1603, 1660, 3038, 3206, 3302, 3850. ¹H NMR δ 1.43 (s, 6H), 2.67 (d, *J* = 13 Hz, 2H), 2.67 (m, 2H), 2.75 (d, *J* = 13 Hz, 2H), 2.93 (m, 2H), 3.32 (d, *J* = 14 Hz, 2H), 3.50 (m, 2H), 3.60 (m, 2H), 3.71 (d, *J* = 13 Hz, 2H), 4.30 (d, *J* = 9 Hz, 2H), 4.34 (d, *J* = 9 Hz, 2H). ¹³C {¹H} NMR δ 20.3, 55.1, 59.4, 64.1, 67.6, 69.7, 85.5.

6aBr₃·H₂O. The trichloride salt of **6a**³⁺ was obtained as a minor component in small quantities together with additional daza·3HCl. The mixture (a few milligrams) was dissolved in H₂O (3 mL), and concd HBr (0.5 mL) was added. Slow evaporation under ambient conditions yielded an orange crystal that could be used for X-ray analysis. UV–vis λ_{max} [nm]: 480, 345.

⁷3⁺.¹⁰ The singly bridged species always eluted together with a large portion of free ligand, and an isolation in pure form proved difficult. The complexes were therefore prepared by selective hydrolysis of dibridged **9**³⁺ (vide infra).

8b[ZnCl₄]Cl·2H₂O. The solid mixture (50 mg) that was obtained from **1b**(CF₃SO₃)₃·2H₂O, method (ii), fraction 4, was dissolved in 3 M HCl, and some solid ZnCl₂ was added. Slow evaporation under ambient conditions yielded yellow crystals suitable for X-ray structure analysis. Anal. Calcd (%) for C₁₅H₃₆Cl₅CoN₆O₃Zn (650.06): C, 27.71; H, 5.58; N, 12.93. Found: C, 27.27; H, 5.43; N, 12.69. IR (cm⁻¹): 500, 514, 524, 530, 537, 546, 559, 584, 651, 695, 781, 818, 853, 897, 925, 981, 1035, 1050, 1065, 1144, 1189, 1257, 1304, 1360, 1378, 1464, 1476, 1500, 1584, 1608, 2978, 3118, 3430, 3493, 3556. UV–vis λ_{max} [nm] (ε[M⁻¹ cm⁻¹]): 470 (162), 345 (182).

9aCl₃·H₂O·HCl. Anal. Calcd (%) for C₁₄H₃₃Cl₄CoN₆O₃ (534.20): C, 31.48; H, 6.23; N, 15.73. Found: C, 31.57; H, 6.14; N, 15.92. IR (cm⁻¹): 700, 757, 802, 824, 897, 960, 1016, 1075, 1130, 1228, 1270, 1433, 1488,

Table 3. Crystallographic Data for 1b[ZnCl₄]Cl·3H₂O,²⁶ 2b[ZnCl₄]Cl·H₂O,²⁶ 3b(ClO₄)₃, 4bCl₃·3H₂O, 6aBr₃·H₂O, 7aBr₃·H₂O, 7b[ZnCl₄]Cl, 8b[ZnCl₄]Cl·2H₂O, 9a[ZnBr₄]Br·H₂O, 9b[ZnCl₄]Cl·H₂O, and 10a[ZnCl₄]Cl·H₂O

	1b ³⁺	2b ³⁺	3b ³⁺	4b ³⁺
chem formula	C ₁₂ H ₃₆ Cl ₅ CoN ₆ O ₃ Zn	C ₁₂ H ₃₂ Cl ₅ CoN ₆ OZn	C ₁₃ H ₃₂ Cl ₃ CoN ₆ O ₁₃	C ₁₄ H ₄₀ Cl ₃ CoN ₆ O ₅
fw	614.02	577.99	645.73	537.80
space group	P2 ₁ 2 ₁ 2 ₁ (No. 19)	P2 ₁ 2 ₁ 2 ₁ (No. 19)	P2 ₁ /n (No. 14)	P $\bar{1}$ (No. 2)
cryst syst	orthorhombic	orthorhombic	monoclinic	triclinic
a, Å	8.94860(10)	8.0404(7)	9.1909(2)	8.0878(4)
b, Å	13.4311(2)	13.3751(11)	21.1145(5)	8.2099(4)
c, Å	20.2761(3)	20.794(2)	12.1697(3)	9.7000(5)
α , deg	90.00	90.00	90.00	75.417(3)
β , deg	90.00	90.00	92.785(1)	85.403(3)
γ , deg	90.00	90.00	90.00	65.570(3)
V, Å ³	2436.98(6)	2236.2(4)	2358.88(10)	567.31(5)
cryst dimensions, mm	0.55 × 0.12 × 0.06	0.53 × 0.19 × 0.14	0.45 × 0.39 × 0.21	0.51 × 0.15 × 0.04
ρ_{calcd} , g cm ⁻³	1.674	1.717	1.818	1.574
μ , cm ⁻¹	2.238	2.427	1.145	1.148
Z	4	4	4	1
diffractometer	Bruker X8	Bruker X8	Bruker X8	Bruker X8
T, K	133(2)	153(2)	153(2)	133(2)
max, min transmission	0.8774, 0.3724	0.7275, 0.3595	0.7950, 0.6268	0.9555, 0.5922
θ_{max}	27.00	26.99	27.00	26.00
abs structure	-0.013(8)	0.018(7)		
data, params	5317, 295	4831, 265	5154, 383	2201, 159
R ₁ [$I > 2\sigma(I)$] ^c	0.0243	0.0212	0.0256	0.0391
wR ₂ (all data) ^d	0.0507	0.0478	0.0653	0.1065
max/min res e-density, eÅ ⁻³	0.349/-0.432	0.417/-0.357	0.520/-0.375	0.955/-0.526
	6a ³⁺	7a ³⁺	7b ³⁺	8b ³⁺
chem formula	C ₁₂ H ₃₀ Br ₃ CoN ₆ O ₂	C ₁₂ H ₃₀ Br ₃ CoN ₆ O ₂	C ₁₄ H ₃₂ Cl ₅ CoN ₆ OZn	C ₁₅ H ₃₆ Cl ₅ CoN ₆ O ₃ Zn
fw	589.08	589.08	602.01	650.05
space group	P2 ₁ /n (No. 14)	P2 ₁ /c (No. 14)	P2 ₁ /n (No. 14)	P2 ₁ 2 ₁ 2 ₁ (No. 19)
cryst syst	monoclinic	monoclinic	monoclinic	orthorhombic
a, Å	9.333(2)	9.5019(4)	10.3321(5)	9.0256(11)
b, Å	15.187(3)	14.7673(5)	14.6219(6)	13.597(2)
c, Å	13.941(3)	13.7535(5)	15.5703(7)	20.494(3)
α , deg	90.00	90.00	90.00	90.00
β , deg	93.84(3)	95.322(2)	105.997(2)	90.00
γ , deg	90.00	90.00	90.00	90.00
V, Å ³	1971.6(7)	1921.54(13)	2261.19(18)	2514.9(6)
cryst dimensions, mm	0.10 × 0.10 × 0.10	0.44 × 0.18 × 0.16	0.35 × 0.28 × 0.11	0.35 × 0.20 × 0.01
ρ_{calcd} , g cm ⁻³	1.985	2.036	1.768	1.717
μ , cm ⁻¹	6.969	7.150	2.404	2.174
Z	4	4	4	4
diffractometer	STOE Stadi 4	Bruker X8	Bruker X8	Bruker X8
T, K	293(2)	153(2)	153(2)	153(2)
max, min transmission	0.5425, 0.5425	0.3941, 0.0917	0.7779, 0.4866	0.9786, 0.5166
θ_{max}	22.50	26.99	27.00	27.00
abs structure				0.001(11)
data, params	2570, 241	4187, 241	4946, 271	5481, 303
R ₁ [$I > 2\sigma(I)$] ^c	0.0425	0.0242	0.0209	0.0322
wR ₂ (all data) ^d	0.0868	0.0538	0.0500	0.0637
max/min res e-density, eÅ ⁻³	0.511/-0.587	1.006/-0.538	0.766/-0.539	0.492/-0.515
	9a ³⁺	9b ³⁺	10a ³⁺	
chem formula	C ₁₄ H ₃₂ Br ₅ CoN ₆ O ₃ Zn	C ₁₆ H ₃₆ Cl ₅ CoN ₆ O ₃ Zn		C ₁₄ H ₃₃ Cl ₆ CoN ₆ O ₃ Zn
fw	856.31	662.06		670.46
space group	P2 ₁ /m (No. 11)	P2 ₁ 2 ₁ 2 ₁ (No. 19)		P2 ₁ 2 ₁ 2 ₁ (No. 19)
cryst syst	monoclinic	orthorhombic		orthorhombic
a, Å	9.1555(4)	12.6507(4)		10.7645(4)
b, Å	11.0171(6)	12.7642(4)		14.2667(6)
c, Å	12.0496(6)	31.0717(11)		15.6069(6)
α , deg	90.00	90.00		90.00
β , deg	93.69(1)	90.00		90.00

Table 3. continued

	9a ³⁺	9b ³⁺	10a ³⁺
γ , deg	90.00	90.00	90.00
V , Å ³	1212.89(10)	5017.3(3)	2396.81(16)
cryst dimensions, mm	0.27 × 0.26 × 0.17	0.71 × 0.46 × 0.10	0.24 × 0.14 × 0.08
ρ_{calcd} , g cm ⁻³	2.345	1.753	1.858
μ , cm ⁻¹	9.938	2.181	2.392
Z	2	8	4
diffractometer	Nonius κ -CCD ^b	Bruker X8	Nonius κ -CCD ^b
T , K	100(2)	123(2)	100(2)
max, min transmission	0.2668, 0.1067	0.8114, 0.3065	0.8094, 0.6175
θ_{max}	30.98	27.00	31.48
abs structure		0.089(4) ^a	0.001(6)
data, params	4022, 253	10 954, 657	7946, 301
R_1 [$I > 2\sigma(I)$] ^c	0.0440	0.0171	0.0251
wR_2 (all data) ^d	0.0959	0.0409	0.0546
max/min res e-density, eÅ ⁻³	0.886/−0.967	0.346/−0.244	0.582/−0.659

^aRacemic twin. ^bRotating anode. ^c $R_1 = \sum ||F_o| - |F_c|| / \sum |F_o|$. ^d $wR_2 = [\sum w(F_o^2 - F_c^2)^2 / \sum wF_o^4]^{1/2}$.

2850, 2990, 3372. ¹H NMR (343 K) δ 2.75 (d, $J = 15$ Hz, 2H), 3.01 (d, $J = 14$ Hz, 2H), 3.13 (m, 2H), 3.24 (m, 2H), 3.43 (br, 2H), 3.55 (m, 2H), 3.62 (m, 2H), 3.88 (m, 2H), 3.94 (m, 2H), 4.38 (d, $J = 11$ Hz, 2H), 4.42 (d, $J = 11$ Hz, 2H), 4.49 (d, $J = 11$ Hz, 2H), 4.90 (d, $J = 11$ Hz, 2H). ¹³C {¹H} NMR (343 K) δ 55.5, 59.3, 60.7, 61.3, 67.6, 82.4, 93.2. UV-vis λ_{max} [nm] (ϵ [M⁻¹ cm⁻¹]): 350 (111), 483 (104).

9a[ZnBr₄]Br·H₂O. 9aCl₃·H₂O·HCl (24 mg, 0.04 mmol) was dissolved in H₂O (2 mL). Solid ZnBr₂ (50 mg) dissolved in 3 M aqueous HBr (5 mL) was added. Slow evaporation under ambient conditions yielded orange crystals suitable for X-ray structure analysis. Anal. Calcd (%) for C₁₄H₃₂Br₃CoN₆O₃Zn (856.28): C, 19.64; H, 3.77; N, 9.81. Found: C, 19.85; H, 3.49; N, 9.81.

9bCl₃·4H₂O. Anal. Calcd (%) for C₁₆H₄₂Cl₃CoN₆O₆ (579.83): C, 33.14; H, 7.30; N, 14.49. Found: C, 32.94; H, 6.95; N, 14.37. IR (cm⁻¹): 713, 827, 918, 982, 1005, 1021, 1042, 1057, 1072, 1108, 1126, 1142, 1158, 1214, 1295, 1389, 1409, 1428, 1491, 1621, 2361, 2837, 2955, 3026, 3104, 3310, 3422. ¹H NMR δ 1.33 (s, 6H), 2.77 (d, $J = 15$ Hz, 2H), 3.07 (d, $J = 14$ Hz, 2H), 3.15 (m, 2H), 3.31 (m, 2H), 3.54 (m, 4H), 3.93 (m, 4H), 4.35 (d, $J = 11$ Hz, 2H), 4.55 (m, 4H), 4.82 (d, $J = 11$ Hz, 2H). ¹³C {¹H} NMR δ 16.6, 55.5, 61.1, 63.1, 68.0, 72.7, 80.6, 92.7. UV-vis λ_{max} [nm] (ϵ [M⁻¹ cm⁻¹]): 352 (115), 486 (107).

9b[ZnCl₄]Cl·H₂O. 9bCl₃·4H₂O (100 mg, 0.17 mmol) was dissolved in 3 M HCl (5 mL). Solid ZnCl₂ (23 mg, 0.17 mmol) was added. Slow evaporation under ambient conditions yielded orange crystals suitable for X-ray analysis. Anal. Calcd (%) for C₁₆H₃₆Cl₅CoN₆O₃Zn (662.07): C, 29.03; H, 5.48; N, 12.69. Found: C, 28.90; H, 5.47; N, 12.58. IR (cm⁻¹): 708, 824, 911, 982, 1005, 1020, 1045, 1131, 1158, 1212, 1256, 1384, 1438, 1492, 2357, 2882, 3078, 3171, 3518.

10a[ZnCl₄]Cl·H₂O. The purple product (15 mg) that was obtained from the tail of the third fraction (Table 2, method (ii)), **1a**³⁺ as the starting material) still contained some dibridged **9a**³⁺ according to NMR spectroscopy. The mixture was dissolved in 3 M HCl (5 mL). Solid ZnCl₂ (35 mg, 0.26 mmol) was added. Slow evaporation yielded a purple crystal suitable for X-ray structure analysis.

Preparation of 7a³⁺ and 7b³⁺ by Partial Hydrolysis of 9a³⁺ and 9b³⁺. 7aBr₃·H₂O. 9aCl₃·H₂O·HCl (200 mg, 0.37 mmol) was dissolved in 50 mL of aqueous 0.5 M KCl. The pH was adjusted to 8 (HEPPS). The progress of the reaction was monitored using cyclic voltammetry. As soon as the signal of **9a**³⁺ had completely disappeared, the reaction was quenched by adding 1 M HCl (400 mL). The solution was sorbed on Dowex 50. The column was washed with H₂O, 0.5 M aqueous HCl, and 1 M HCl, and a fraction of pure **7a**³⁺ was then eluted with aqueous 3 M HCl. The orange solution was evaporated to dryness. The resulting solid was dissolved again in 3 M HBr. Slow evaporation under ambient conditions yielded orange-red crystals suitable for X-ray structure analysis (60 mg, 0.10 mmol, 27%). Anal. Calcd (%) for C₁₂H₃₀Br₃CoN₆O₂ (589.05): C, 24.47; H, 5.13; N, 14.27. Found: C, 24.89; H, 5.10; N, 14.21. IR (cm⁻¹): 510, 523, 530, 547, 574, 588, 613,

688, 717, 765, 841, 885, 898, 931, 960, 979, 991, 1017, 1031, 1049, 1064, 1115, 1138, 1162, 1224, 1271, 1287, 1322, 1348, 1362, 1381, 1434, 1468, 1487, 1556, 1582, 1622, 2737, 2857, 3008, 3086, 3417, 3472. ¹H NMR (333 K) δ 2.72 (d, 2H), 2.76 (d, 1H), 2.96 (d, $J = 14$ Hz, 1H), 3.00–3.15 (m, 3H), 3.23 (m, 1H), 3.38 (m, 1H), 3.42 (m, 1H), 3.55 (m, 4H), 3.59 (m, 1H), 3.77–3.96 (m, 3H), 4.38–4.50 (m, 3H), 4.86 (d, $J = 11$ Hz, 1H). ¹³C {¹H} NMR (333 K) δ 55.2, 56.2, 56.6, 57.3, 58.8, 61.0, 61.1, 61.9, 62.3, 67.9, 82.7, 93.7. UV-vis λ_{max} [nm] (ϵ [M⁻¹ cm⁻¹]): 480 (107), 347 (95).

7b[ZnCl₄]Cl. 9bCl₃·4 H₂O (24 mg, 0.03 mmol) was dissolved in D₂O (4 mL), and the pH* was adjusted to 8.0 (0.025 M borax buffer).¹² From this solution, an aliquot (600 μ L) was transferred into an NMR tube, and the formation of **7b**³⁺ was monitored by ¹H NMR measurements. As soon as the signals of **9b**³⁺ (methyl group) had completely disappeared, the reaction was quenched by adding 1 M HCl, and some solid ZnCl₂ was added. Slow evaporation under ambient conditions yielded orange crystals suitable for X-ray structure analysis. The crystals, which tend to effloresce slowly, were dried in vacuo (8 mg, 39%). Anal. Calcd (%) for C₁₄H₃₂Cl₅CoN₆OZn (602.02): C, 27.93; H, 5.36; N, 13.96. Found: C, 27.51; H, 5.73; N, 13.74. IR (cm⁻¹): 624, 683, 702, 827, 859, 918, 954, 988, 1007, 1031, 1052, 1072, 1131, 1264, 1295, 1361, 1392, 1435, 1472, 1489, 1600, 2284 (br), 2757, 2866, 2981, 3055, 3155. ¹H NMR δ 1.32 (s, 3H), 1.43 (s, 3H), 2.74 (m, 2H), 2.79 (d, $J = 14$ Hz, 1H), 3.01 (d, $J = 13$ Hz, 1H), 3.06 (m, 1H), 3.10 (m, 1H), 3.15 (m, 1H), 3.25 (m, 1H), 3.37 (m, 1H), 3.49 (m, 3H), 3.59 (m, 1H), 3.80 (m, 1H), 3.89 (m, 2H), 4.38 (br, 1H), 4.47 (br, 1H), 4.54 (br, 1H), 4.82 (d, 1H). ¹³C {¹H} NMR δ 16.7, 20.3, 55.1, 56.2, 56.5, 60.6, 62.6, 64.4, 66.8, 67.2, 68.3, 72.3, 81.0, 93.3. UV-vis λ_{max} [nm] (ϵ [M⁻¹ cm⁻¹]): 478 (91), 345 (94).

Single-Crystal X-ray Diffraction Studies. Details of data collection and structure solution are listed in Table 3. Graphite monochromated Mo K α radiation ($\lambda = 0.71073$ Å) was used throughout. The structures were solved by the heavy atom method (**1b**[ZnCl₄]Cl·3H₂O, **3b**(ClO₄)₃, and **4b**Cl₃·3H₂O) or direct methods (all other structures) using SHELXS-97 and were refined by full-matrix least-squares calculations on F^2 (SHELXL-97).²² Anisotropic displacement parameters were refined for all nonhydrogen atoms. A numerical absorption correction (face-indexed) was applied to **9a**[ZnBr₄]Br·H₂O and **10a**[ZnCl₄]Cl·H₂O, and an empirical correction was applied to **6a**Br₃·H₂O. A semiempirical correction method (multiscan) was applied to all other data sets. Puckering parameters²³ were calculated using the computer program PLATON.²⁴

Disorder. Two of the three perchlorate anions (Cl1, O1–O4/Cl3, and O9–O12) in **3b**(ClO₄)₃ proved to be disordered and were refined in each case as a major (A, 89/81%) and a minor (B, 11/19%) component using the SAME and EADP instructions of SHELXL. Atoms Cl2 and O3W in **4b**Cl₃·3H₂O were located on the same position (EXYZ) with occupancies of 50% each. Both atoms were refined with equal displacement parameters (EADP). In **9a**[ZnBr₄]Br·H₂O, the

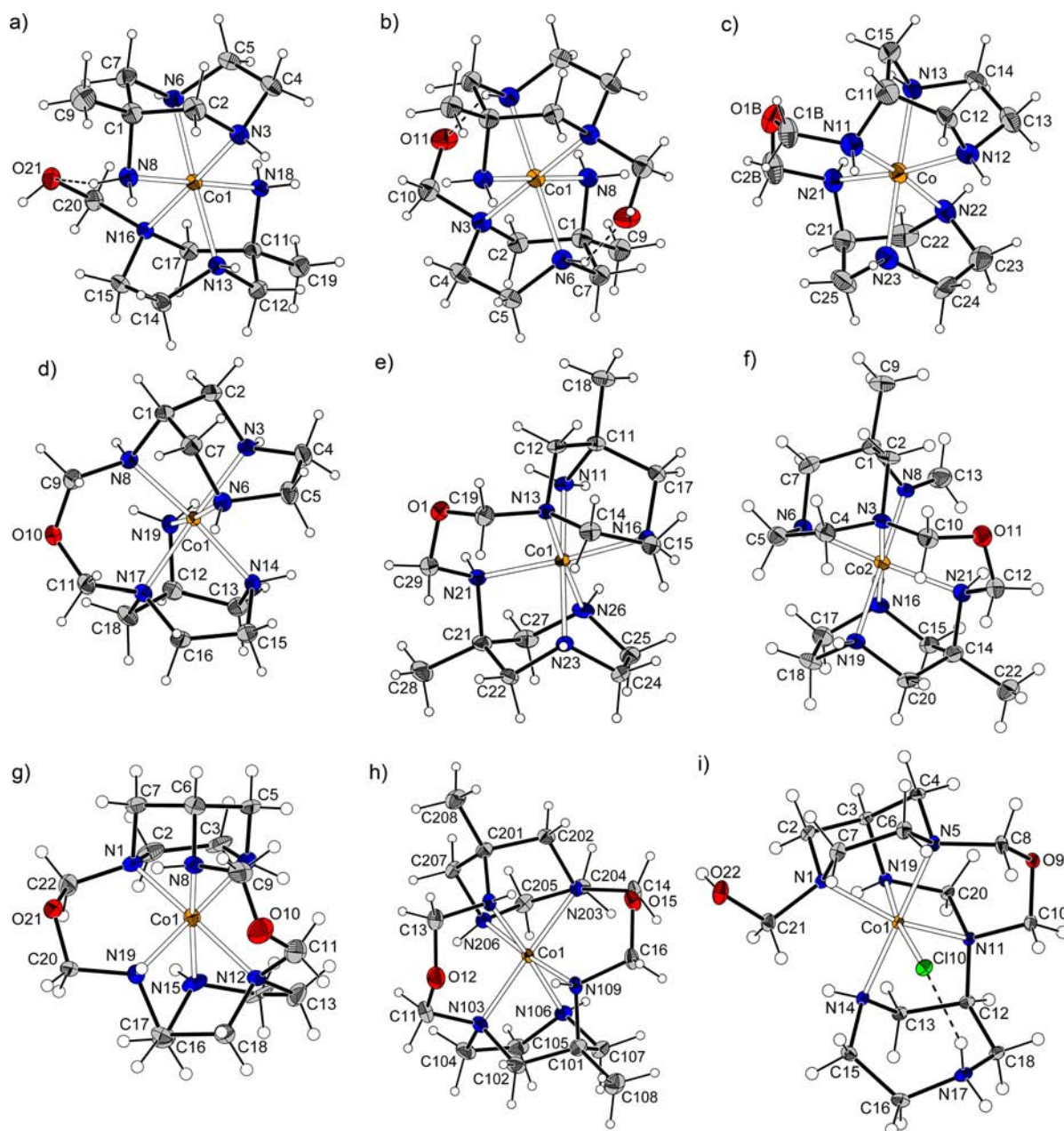


Figure 1. Molecular structure and numbering scheme of (a) $3b^{3+}$, (b) $4b^{3+}$, (c) $6a^{3+}$, (d) $7a^{3+}$, (e) $7b^{3+}$, (f) $8b^{3+}$, (g) $9a^{3+}$, (h) $9b^{3+}$, and (i) $10a^{3+}$. The displacement ellipsoids are drawn at the 50% probability level; hydrogen atoms are shown as spheres of arbitrary size. Hydrogen bonds are displayed as dashed lines. In panel h, only one of the two crystallographically independent $9b^{3+}$ cations (the one without disorder) is displayed, the other cation is shown in Figure S2 (Supporting Information).

metal center Co1 as well as C9 are located on a crystallographic mirror plane. Consequently, the ligand of the metal complex is disordered over two sites with occupancies of each 50%. An alternative refinement as merohedral twin in the space group $P2_1$ did not improve the quality and was therefore discarded. In $9b[ZnCl_4]Cl \cdot H_2O$, one of the N–CH₂–O–CH₂–N bridges is disordered and was described as a major component (A, 74%) adopting a cisoid and a minor component (B, 26%) adopting a transoid conformation with regard to the H–N–C–O torsional angle (Figure S2). The Flack parameter²⁵ of this structure refined to a value of 0.089(4), indicating the formation of an inversion twin. As a consequence, the TWIN option of SHELXL was used in the final refinement. In agreement with the Flack parameter, the BASF parameter was found to be 9%.

Treatment of Hydrogen Atoms. Calculated positions (riding model) were usually used for H(-C) atoms. However, no optimal positions were obtained for the hydrogen atoms bound to C14, C21B, C30S, and C40S

of $9b[ZnCl_4]Cl \cdot H_2O$. Their positional parameters were thus refined freely using restraints of 0.99 Å for the C21B–H distances. The H(-N) positions of $9a[ZnBr_4]Br \cdot H_2O$ were calculated, and the H(-O) atoms of the corresponding water molecule as well as the H(-O) atoms of the three water molecules in $4bCl_3 \cdot 3H_2O$ could not be located and were not considered in the refinement. The H(-N) and the H(-O) atoms in $10a[ZnCl_4]Cl \cdot H_2O$ were located in a difference Fourier map and were refined isotropically. The positional parameters of all other O- and N-bonded hydrogen atoms were refined using isotropic displacement parameters that were set to $1.5 \times U_{eq}$ of the pivotal O atom and $1.2 \times U_{eq}$ of the pivotal N atom, respectively. In addition, restraints of 0.84 and 0.88 Å (0.82 and 0.86 Å at 293 K) were used for the O–H and N–H distances, respectively.

RESULTS

Preparation, Product Distribution, and Characterization. The daza and Medaza complexes 1^{3+} and 2^{3+} have been prepared by the usual aerial oxidation of a Co^{II} precursor.^{7,8} Similar to bis-dapi complexes,⁴ they adopt either a chiral C_2 -symmetric cis (1^{3+}) or an achiral C_{2h} -centrosymmetric trans (2^{3+}) configuration. Both diastereomers were subjected to the bridging reaction, which was performed in acetonitrile by the action of paraformaldehyde and triethylamine. The complexes were supplied as trifluoromethanesulfonate salts because they assured the required solubility in the nonprotic medium.²⁰ In all four cases, the resulting product was found to be an intricate mixture of several components, which could be only partially resolved by chromatography on a 2 m Sephadex column. Subsequent crystallization experiments yielded single crystals of hemiaminals $3b^{3+}$ and $4b^{3+}$ and of species with one ($6a^{3+}$, 7^{3+} , $8b^{3+}$, and $10a^{3+}$) or two (9^{3+}) oxidimethaneamine bridges (Scheme 2). The molecular structure of these complexes was elucidated by an X-ray diffraction study (Figure 1).²⁶ Dibridged 9^{3+} was provided in sufficient quantities to allow NMR measurements. The NMR data of singly bridged 7^{3+} were obtained from samples that have been prepared by partial hydrolysis of 9^{3+} (vide infra). Considering these NMR characteristics, further species (hemiaminal $5b^{3+}$ and diimine $11b^{3+}$) could be identified in the product mixtures of some of the fractions collected in the chromatographic procedure.²⁷ However, a variety of additional components still remains unknown.

In an early stage of this study, a meaningful interpretation of the product distribution was rather puzzling. We observed a poor reproducibility and concluded that the product distribution must strongly depend on some specific, unidentified parameters. A thorough and systematic variation of the reaction conditions, such as the order of addition of the ingredients, the presence or absence of some small traces of triflic acid, or the water content, have been undertaken.²¹ The experiments revealed that the amount of water is particularly crucial. Some remaining moisture has a dramatic influence on the reaction rate²⁸ and product distribution: if carefully dried materials were used, then the reaction mixture first adopted a light-gray color, then darkened slowly, and finally, after about 30 min, a strongly colored, almost black slurry formed. However, in the presence of some traces of water, the strongly colored slurry was almost immediately obtained, and the conversion appears to be completed within a few seconds. A representative selection of such experiments is shown in Table 2, and the principal results can be summarized as follows.

- (1) In all reactions, the main product was dibridged 9^{3+} ,¹⁰ which was isolated in quantities of 41–85%. Singly bridged 7^{3+} formed, if at all, to a much smaller extent (<10%). In all four complexes, the oxidimethaneamine bridges connect a primary amino group of one diazepan-amine frame with a secondary amino group of the other (prim–sec bridging).
- (2) In the fast runs (method ii)²⁸ taking place in the presence of moisture, some additional byproducts could be identified. Formation of the prim–prim-bridged species $6a^{3+}$ could only be observed occasionally in the reaction with the daza complexes $1a^{3+}$ and $2a^{3+}$. Its amount was generally low, and it was only once formed in sufficient quantities to allow the growth of a single crystal for structure analysis. Another occasionally isolated daza derivative, which was again obtained in small quantities,

was the rather exotic $10a^{3+}$, where one of the secondary amino groups is detached from Co^{III} , protonated, and hydrogen bonded to a coordinated chloride ligand. Complex $10a^{3+}$ contains one prim–sec-oxidimethaneamine bridge and an additional prim–sec-methylene bridge, forming a four-membered chelate ring.²⁹ Furthermore, one of the endocyclic nitrogen donor carries a pendant $\text{CH}_2\text{--OH}$ substituent.³⁰ The Medaza complex $1b^{3+}$ yielded the singly bridged, monomethylideneimine species $8b^{3+}$ and the nonbridged, bis-methylideneimine species $11b^{3+}$ as byproducts.

- (3) In all bridged complexes ($6a^{3+}$, 7^{3+} , $8b^{3+}$, 9^{3+} , and $10a^{3+}$),¹⁰ the two 1,4-diazepan-6-amine frames exclusively exhibited a cis configuration (Figure 1) regardless of whether a cis- (1^{3+}) or trans- (2^{3+}) configured template was used as starting material! Obviously a rearrangement from trans to cis must occur during the bridging process.
- (4) In the slow reaction²⁸ (i.e., in the absence of water, method i) the cis and trans daza derivatives $1a^{3+}$ and $2a^{3+}$ react equally, yielding only the prim–sec-bridged species $7a^{3+}$ and $9a^{3+}$. Additional byproducts were not isolated. However, in the slow reaction of the *trans*-Medaza derivative $2b^{3+}$ (method iii) a series of hemiaminals ($3b^{3+}$ – $5b^{3+}$) with one or two pending carbinolamino groups³⁰ were formed and could be isolated and characterized. Notably, in these hemiaminals, the trans orientation of the two Medaza frames is retained.
- (5) The fractions with the singly bridged species $6a^{3+}$ and 7^{3+} contained a considerable amount of protonated free ligand H_3L^{3+} or $\text{H}_3\text{MeL}^{3+}$. Because the starting materials did not contain any free ligand at all, the rather large amount observed must be liberated either during the course of the bridging reaction or during work up.
- (6) In most of the experiments, some very minor bands were observed beside the main products. The amount of these byproducts was too marginal for a subsequent isolation and characterization. For some of them, the presence of Co^{2+} could be verified.

Solution Properties: Conformational Equilibria, Redox Chemistry, and Hydrolysis. The NMR properties of the nonbridged 1^{3+} and 2^{3+} have been reported in our previous papers.^{7,8} Their interpretation is straightforward. However, for the daza derivatives $7a^{3+}$ and $9a^{3+}$, the observations were rather confusing at first glance. The ^1H NMR spectra of both complexes exhibited some broad and unresolved signals (Figure 2). Such observations are normally characteristic of H(–N–Co) resonances, and heating in D_2O usually results in a complete disappearance of these signals owing to H versus D exchange. This was, however, not verified for $7a^{3+}$ and $9a^{3+}$. Instead, sharp signals were found at elevated temperature, and 2D C–H COSY experiments unambiguously established that all of these resonances belong to carbon-bonded hydrogen atoms, with the particularly broad signals belonging to the CH_2 hydrogen atoms of the oxidimethaneamine bridges (Figure S4).³¹ We thus attribute these observations to a conversion of different conformers with coalescence close to room temperature. A similar temperature-dependent line broadening has also been observed in the ^{13}C NMR spectra. After recognition of this particular behavior, the interpretation of the NMR data is again straightforward, with the singly bridged C_1 -symmetric $7a^{3+}$ and dibridged C_2 -symmetric $9a^{3+}$ exhibiting 12 and 7 resonances in the ^{13}C NMR spectrum, respectively. For the Medaza derivatives

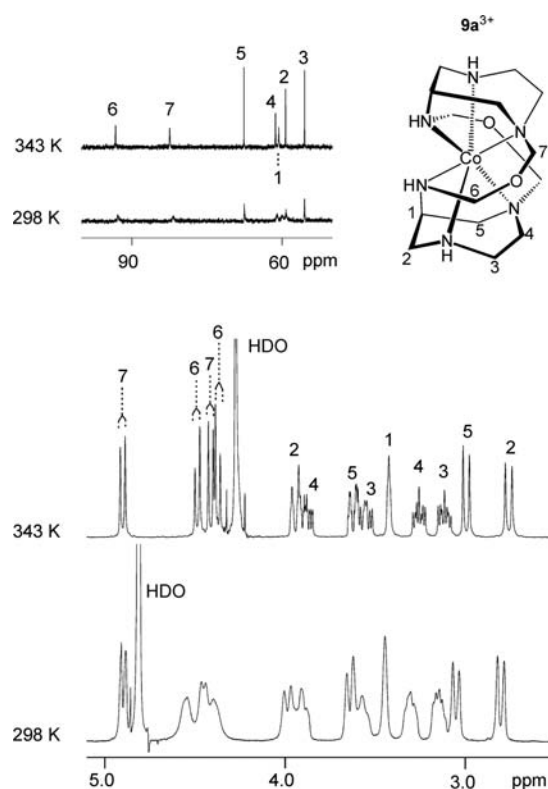


Figure 2. ^1H and ^{13}C NMR spectra of 9a^{3+} (D_2O , 0.1 M DCl) at the indicated temperatures.

7b^{3+} and 9b^{3+} , a related dynamic behavior was also observed. However, in comparison to the daza derivatives, the effect was much less pronounced.

The redox potentials of parent $1\text{a}^{3+/2+}$ and $1\text{b}^{3+/2+}$ are already known.⁸ Cyclic voltammograms of dibridged 9^{3+} were measured in a slightly acidic aqueous solution (pH 5). Under these conditions, the complexes proved to be stable in the Co^{II} and Co^{III} stage and revealed quasi-reversible redox behavior. For all samples, the peak current of the oxidation and reduction wave depended linearly on the square root of the scan rate, as expected for a diffusion-controlled process. However, in alkaline media, the samples were not stable, and the cyclic voltammograms indicated transformation into new Co complexes, which in turn showed again quasi-reversible redox behavior (Figure 3). The new complexes experienced further, but much slower, decomposition. The reduction potentials of the final products agreed with the values observed for the nonbridged $1^{3+/2+}$ couples. Similarly, the redox potentials of the intermediates concurred with the singly bridged 7^{3+} . As shown in Table 4, simple daza and Medaza complexes of Co^{III} are weaker oxidizing agents than the corresponding singly bridged derivatives, and these in turn are weaker oxidizing agents than the dibridged complexes. ^1H and ^{13}C NMR measurements of 9^{3+} in slightly alkaline D_2O solutions (pH* ~ 9)¹² confirmed a rapid transformation of the dibridged species into the singly bridged derivatives and a subsequent, slower transformation to the nonbridged complexes 1^{3+} (Figure 4).

Molecular Mechanics Calculations. To shed more light on the specific steric conditions in the various structures, and in particular on the nonobservance of any trans-configured bridged species, molecular mechanics calculations have been performed for 1^{3+} and 2^{3+} and for several singly and dibridged derivatives thereof. The strain energies of selected relevant structures are

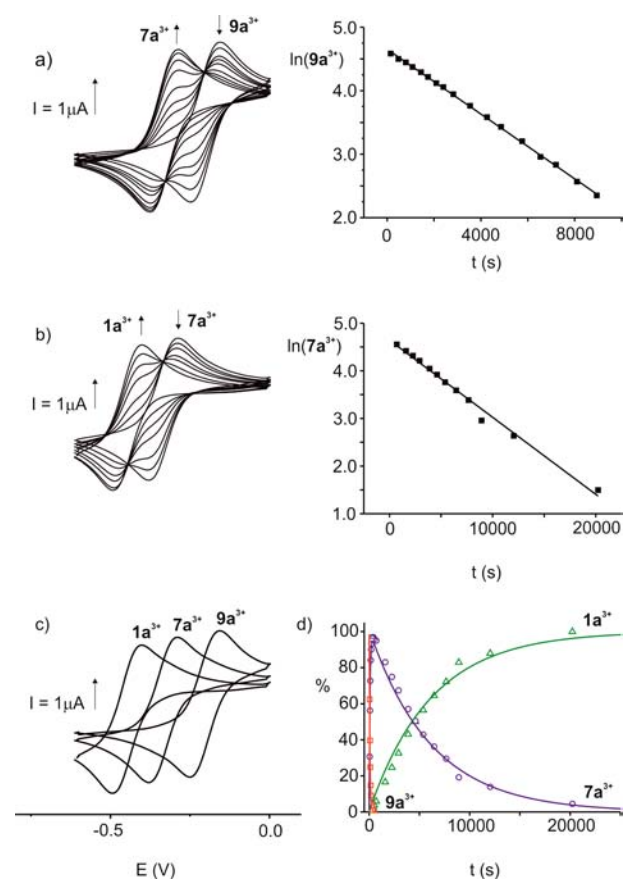


Figure 3. $9\text{a}^{3+} \rightarrow 7\text{a}^{3+} \rightarrow 1\text{a}^{3+}$ transformation observed by CV measurements at 25°C (2 M KCl). The individual transformations $9\text{a}^{3+} \rightarrow 7\text{a}^{3+}$ and $7\text{a}^{3+} \rightarrow 1\text{a}^{3+}$ together with the corresponding first-order behavior are depicted. (a) pH 7.52 and (b) pH 9.5. Cyclic voltammograms of the pure components at pH 8.0 (c). Synopsis of the concentrations as a function of time at pH 9.5 (d). In panel d, the curves represent the best fit (least-squares) according to eqs 1 and 3'.

Table 4. Survey of the Mean Co–N Distances, Maximum Absorption (λ_{max}) of the $A_{1g}-T_{1g}$ Transitions, and Redox Potentials (vs SHE) of $1^{3+/2+}$ and Bridging Products $6\text{a}^{3+/2+}$, $7\text{a}^{3+/2+}$, $8\text{b}^{3+/2+}$, and $9\text{a}^{3+/2+}$

	mean $d(\text{Co}-\text{N})$ (Å)	λ_{max} ($A_{1g}-T_{1g}$) (nm)	E° ($\text{Co}^{\text{III}}/\text{Co}^{\text{II}}$) (V)
nonbridged			
1a^{3+}	1.976 ^a	470 ^a	-0.23 ^b
1b^{3+}	1.966 ^c	472 ^d	-0.27 ^e
singly bridged			
6a^{3+}	1.985	480	
7a^{3+}	1.978	480	-0.12
7b^{3+}	1.981	478	-0.15
singly bridged, monomethylideneimine			
8b^{3+}	1.980	470	
dibridged			
9a^{3+}	1.989	483	+0.01
9b^{3+}	1.985	486	-0.02

^aFrom ref 7. ^bRef 7 reports a value of -0.21 V. The deviation obviously originates from the different ionic strength. ^c*cis*-[Co-(Medaza)₂][ZnCl₄].Cl·3H₂O (this work). The mean distance reported in ref 8 is slightly larger. ^dFrom ref 8. ^eRef 8 reports a value of -0.24 V. The deviation obviously originates from the different ionic strength.

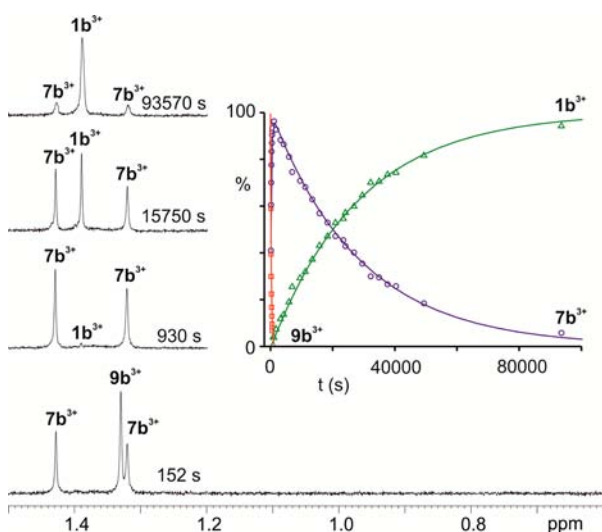


Figure 4. $9b^{3+} \rightarrow 7b^{3+} \rightarrow 1b^{3+}$ transformation observed by ^1H NMR measurements at 21 °C and $\text{pH}^* 8.9$ (2 M KCl).¹² The methyl region is shown, where $9b^{3+}$ and $1b^{3+}$ display one and $7b^{3+}$ displays two resonances for the methyl groups.³⁵ The curves represent the best fit (least-squares) according to eqs 1 and 3'.

collected in Table 5 (the results for all 54 calculated structures are supplied in Table S1). A comparison of the structural parameters with experimental findings as obtained from crystal structure analysis of 1^{3+} , 2^{3+} , $6a^{3+}$, 7^{3+} , and 9^{3+} is shown in Table 6. The calculations are based on the following considerations. (a) Only bridges between two exocyclic or an exocyclic and an endocyclic nitrogen donor were taken into account (see the mechanism outlined in Scheme 1). (b) Bridging interactions involving a primary amino group generate an additional stereogenic nitrogen atom that may adopt either an *R* or an *S* configuration.^{17,32} Bearing in mind that the *cis*-[Co(daza)₂] scaffold itself is chiral with a clockwise (*C*) or an anticlockwise (*A*) sequence of the hexamine donor set,³³ different diastereomers such as *C(S,S)* or *C(R,R)* must be accounted for. (c) Conformational flexibility within the oxidimethaneamine bridge (as shown by the NMR measurements) gives rise to different conformations that were identified using puckering parameters, as defined by Cremer and Pople (Table S2).²³ In addition, we paid attention to the $\text{H}-\text{N}_{\text{exo}}-\text{C}-\text{O}$ and $\text{C}_{\text{propylene}}-\text{N}_{\text{endo}}-\text{C}-\text{O}$ torsional angle θ , which may adopt either a cisoid or transoid geometry (Table 6).³⁴

Although the calculated Co–N distances are in general slightly underestimated by the MOME program (Table 6),¹⁷ the observed trend (i.e., a slight increase of the mean Co–N bond distances with an increasing number of bridges) is well reproduced. Moreover, the calculations confirmed that the species that were obtained in the synthetic procedure, namely, the singly bridged $6a^{3+}$ and 7^{3+} as well as dibridged 9^{3+} represent low-energy structures indeed and that formation of an oxidimethaneamine bridge is in general much more favorable for species with the two diazepane frames having a *cis* orientation. In addition, the most stable conformation of the oxidimethaneamine bridge is in general well reproduced by the MOME calculations (Figure 5).

Kinetics of Bridge Cleavage. The above-mentioned CV experiments represent a convenient method for an explicit registration of the time course of bridge cleavage (Figure 3). The decomposition process of the Medaza derivative $9b^{3+}$ could also be studied by ^1H NMR spectroscopy (Figure 4) by monitoring the signals of the additional methyl groups, which appear as

sharp, simple singlets.³⁵ Both methods gave consistent results.³⁶ ^1H NMR spectroscopy is, however, not the method of choice for a quantitative examination of daza derivatives $1a^{3+}$, $7a^{3+}$, and $9a^{3+}$ because the ^1H resonances of the diazepane ring appeared as poorly resolved, overlapping signals with marginal alteration in the course of the reaction. For similar reasons, bridge cleavage cannot be followed by vis spectroscopy because the difference in λ_{max} of the various species is rather small (Table 4).

The kinetics of the entire degradation reaction $9^{3+} \rightarrow 1^{3+}$ were studied at a constant ionic strength (2 M KCl) in aqueous solution. Suitable buffers were used to ensure constant OH^- concentration in the range $6.4 \leq \text{pH} \leq 11.6$. The observation of two oxidation and two reduction waves for each step with isosbestic points (Figure 3) is in agreement with a simple two-step transformation, $9^{3+} \rightarrow 7^{3+} \rightarrow 1^{3+}$. Singly bridged 7^{3+} appear to be the sole intermediates that are formed in significant concentration. At pH 7.5, the complete conversion of 9^{3+} to 7^{3+} took hours. As already mentioned, the cleavage of the second bridge occurred at a significantly slower rate, and the subsequent degradation of 7^{3+} to nonbridged 1^{3+} required a few weeks. The two decomposition steps are thus well separated, and it is possible to obtain solutions where the singly bridged intermediates strongly predominate. Assuming pseudo-first-order kinetics with corresponding rate constants k_1 and k_2 for the two consecutive steps, the integrated rate laws read as follows

$$[9^{3+}](t) = [9^{3+}]_0 e^{-k_1 t} \quad (1)$$

$$[7^{3+}](t) = [9^{3+}]_0 k_1 (k_2 - k_1)^{-1} (e^{-k_1 t} - e^{-k_2 t}) \quad (2)$$

$$[1^{3+}](t) = [9^{3+}]_0 \{1 + (k_2 e^{-k_1 t} - k_1 e^{-k_2 t}) (k_1 - k_2)^{-1}\} \quad (3)$$

where $[9^{3+}]_0 = [9^{3+}] + [7^{3+}] + [1^{3+}]$ stands for the molar concentration of 9^{3+} at $t = 0$. The rate constant k_1 can be evaluated directly. If we further propose $k_1 \gg k_2$, then eq 3 reduces to

$$[1^{3+}](t) = [9^{3+}]_0 (1 - e^{-k_2 t}) \quad (3')$$

and k_2 can again be derived by linear regression analysis of the $\ln([1^{3+}]/[9^{3+}]_0)$ versus t curve. A linear dependence of $\ln([9^{3+}]/[9^{3+}]_0)$ or $\ln(1 - [1^{3+}]/[9^{3+}]_0)$ on t was indeed observed (Figure 3 and Table 1). Moreover, the half-lives ($t_{1/2} = k_1^{-1} \ln 2$; $i = 1, 2$) of the two reaction steps, as expected for a first-order reaction, did not depend on $[9^{3+}]_0$. The corresponding values of k_1 and k_2 for different pH values are collected in Table 1. The ratio k_1/k_2 was found to be $67 \pm 18 \text{ s}^{-1}$ for the daza and $117 \pm 15 \text{ s}^{-1}$ for the Medaza derivatives, and the precondition for our evaluation, viz. $k_1 \gg k_2$, is thus reasonably well fulfilled. The maximum concentration $[7^{3+}]_{\text{max}}$ of intermediate 7^{3+} that forms at the time t_{max} can be derived from eq 2 as

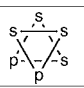
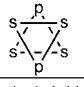
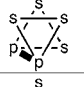
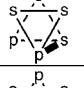
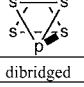
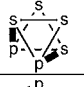
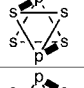
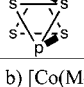
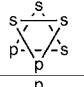

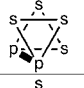
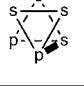
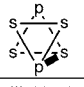
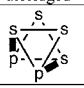
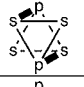
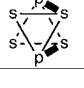
$$t_{\text{max}} = (k_1 - k_2)^{-1} \ln(k_1/k_2) \quad (4)$$

$$[7^{3+}]_{\text{max}} = [9^{3+}]_0 (k_2/k_1)^{k_2/(k_1-k_2)} \quad (5)$$

For the degradation of the daza derivatives at pH 9.5, for instance, $t_{\text{max}} = 326 \text{ s}$ and $[7a^{3+}]_{\text{max}} = 95\%$ of $[9a^{3+}]_0$. Similarly, for the Medaza derivatives at pH 8.9, $t_{\text{max}} = 20 \text{ min}$ and $[7b^{3+}]_{\text{max}} = 96\%$ of $[9b^{3+}]_0$. These values agree well with our observations (Figures 3 and 4).

In the range $6.4 < \text{pH} < 10.5$, $\log(k_i)$ depended linearly on pH with a slope close to unity (Figure 6), and the rate constant can be formulated as

Table 5. Strain Energies (kJ mol⁻¹) as Calculated by Molecular Mechanics Calculations

a) [CoL ₂] ³⁺ and selected bridged derivatives ^a			Bond Def.	Non-Bond. Interactions	Valence Angle Def.	Torsion Angle Def.	Total Strain
	<i>cis</i> -[CoL ₂] ³⁺	1a ³⁺ C ₂	10.14	49.52	18.98	40.41	119.05
	<i>trans</i> -[CoL ₂] ³⁺	2a ³⁺ C _{2h}	11.38	56.09	17.50	40.98	125.95
singly bridged							
	C(S _o S _i) ^c	6a ³⁺ C ₁	12.42	59.38	28.69	48.63	149.12
	C(S _o S _i)	C ₂	18.07	77.10	27.24	51.36	173.77
	C(R _o S _i)	C ₁	17.37	78.02	33.80	51.26	180.44
	C(R _o R _c)	7a ³⁺ C ₁	12.88	61.08	26.07	45.49	145.52
	C(R _o R _i)	C ₁	16.73	70.77	42.58	51.18	181.27
	C(R _i R _i)	C ₁	13.62	63.45	25.61	50.74	153.41
	R _i S _i	C ₁	15.67	71.70	28.15	49.82	165.33
	R _o S _i	C ₁	17.62	75.64	33.32	40.49	167.07
dibridged							
	C(R _o R _c ; R _o R _c)	9a ³⁺ C ₂	15.88	71.84	32.78	53.20	173.70
	C(R _o R _c ; R _i R _i)	C ₁	16.81	74.45	33.11	57.89	182.27
	C(R _i R _i ; R _i R _i)	C ₂	17.86	77.32	34.17	61.37	190.73
	R _i S _i ; S _i R _i	C _i	21.81	95.82	41.99	57.66	217.28
	R _i S _i ; S _o R _i	C ₁	24.58	102.98	49.14	49.80	226.49
	R _o S _i ; S _o R _i	C _i	27.38	110.55	58.74	43.66	240.33
	R _o S _i ; R _o S _i	C ₂	24.20	88.13	47.74	42.32	202.39
	R _o S _i ; R _i S _i	C ₁	22.75	87.27	43.92	50.47	204.40
	R _i S _i ; R _i S _i	C ₂	21.27	85.41	38.89	59.79	205.36
b) [Co(MeL) ₂] ³⁺ and selected bridged derivatives ^a							
Complex ^b			Bond Def.	Non-Bond. Interactions	Valence Angle Def.	Torsion Angle Def.	Total Strain
	<i>cis</i> -[Co(MeL) ₂] ³⁺	1b ³⁺ C ₂	10.64	55.12	19.10	40.61	125.47
	<i>trans</i> -[Co(MeL) ₂] ³⁺	2b ³⁺ C _{2h}	11.85	61.75	17.73	41.22	132.55
singly bridged							
	C(S _o S _i) ^c	C ₁	13.66	67.25	30.99	49.36	161.27
	C(S _o S _i)	C ₂	19.88	85.15	29.66	50.48	185.17
	C(R _o S _i)	C ₁	18.64	84.47	35.64	51.87	190.61
	C(R _o R _c)	7b ³⁺ C ₁	13.66	67.01	26.82	45.52	153.01
	C(R _o R _i)	C ₁	17.31	76.17	43.75	51.03	188.26
	C(R _i R _i)	C ₁	14.60	70.15	27.87	50.62	163.23
	C(S _i R _c)	C ₁	17.05	78.97	44.61	51.51	192.13
	R _i S _i	C ₁	16.61	78.22	29.70	50.42	174.95
	R _o S _i	C ₁	18.27	80.99	34.51	40.60	174.36
dibridged							
	C(R _o R _c ; R _o R _c) ^d	9b ³⁺ C ₂	17.11	78.86	33.78	53.68	183.43
	C(R _o R _c ; R _i R _i) ^d	9b ³⁺ C ₁	17.60	81.24	37.10	57.37	193.31
	C(R _i R _i ; R _i R _i)	C ₂	18.33	84.13	38.27	62.84	203.57
	R _i S _i ; S _i R _i	C _i	23.76	104.17	44.06	58.16	230.15
	R _i S _i ; S _o R _i	C ₁	26.26	110.01	50.90	49.98	237.15
	R _o S _i ; S _o R _i	C _i	29.06	116.66	60.20	43.08	249.01
	R _o S _i ; R _o S _i	C ₂	25.15	95.59	50.03	42.42	213.19
	R _o S _i ; R _i S _i	C ₁	24.18	95.28	46.84	51.15	217.46
	R _i S _i ; R _i S _i	C ₂	22.92	94.19	42.19	61.48	220.77

^aOnly bridged species with a total strain energy of less than 40 kJ mol⁻¹ above the most favorable representative of each category are shown. A compilation of all calculated structures is given in Table S1. Bold numbers refer to observed species. ^bIn the schematic representations shown in the first column, exocyclic (formerly primary) and endocyclic (formerly secondary) amino groups of the diazepane frames are abbreviated with p and s, respectively. The oxidimethaneamine bridges are indicated by bold straps. In the second column, the configuration (R or S) of the stereogenic nitrogen atoms are listed. The first label always refers to the exocyclic (p) nitrogen atom. The labels *c* (cisoid) and *t* (transoid) refer to the H–N–C–O (N_{exo}) or C_{propylene}–N–C–O (N_{endo}) torsional angles.³⁴ The *cis*-configured complexes all have a clockwise (C) absolute configuration.³³ ^cIn this particular case, C(S_oS_i) and C(S_oS_i) represent the same structure. The average symmetry for a rapid equilibrium between the two forms is C₂. ^dIn the crystal structure of **9b**[ZnCl₄]Cl·H₂O, one of the two crystallographically independent cations adopts a C(R_oR_c; R_oR_c) structure, whereas the second

Table 5. continued

cation was disordered with the major component adopting again a $C(R_p R_i; R_p R_i)$ structure and minor component adopting a $C(R_p R_i; R_p R_i)$ structure.

Table 6. Synopsis of the Structural Parameters of L and MeL Complexes and Their Bridged Derivatives as Obtained from the Crystal Structure Analysis (Table 3)^a

	mean M–N _{exo} distance (Å)	mean M–N _{endo} distance (Å)	N _{endo} –C–C–N _{endo} torsional angle (deg)	H–N _{exo} –C–O/C _{propylene} –N _{endo} –C–O torsional angle (deg)
1a ³⁺	1.959 ^b (1.947)	1.985 ^b (1.962)	0.5, 4.9 ^b (2.2, 2.2)	
2a ³⁺	1.950 ^b (1.950)	1.980 ^b (1.965)	0.3, 6.3 ^b (0.0, 0.0)	
1b ³⁺	1.968 ^c (1.947)	1.966 ^c (1.961)	3.7, 6.5 ^c (2.2, 2.2)	
2b ³⁺	1.953 ^c (1.950)	1.987 ^c (1.964)	4.2, 5.2 ^c (0.1, 0.0)	
3b ³⁺	1.946	1.996	6.6, 6.9	
4b ³⁺	1.952	2.002	7.3	
6a ^{3+^d}	1.973 (1.950)	1.991 (1.968)	1.2, 1.3 (0.7, 3.1)	87.1, 147.7 (85.0, 152.4)
7a ³⁺	1.953 (1.953)	1.990 (1.967)	1.2, 8.2 (2.2, 6.9)	83.4/68.5 (83.3/69.3)
7b ³⁺	1.962 (1.954)	1.991 (1.966)	3.9, 4.6 (4.3, 8.7)	82.7/73.5 (81.1/70.3)
8b ³⁺	1.948	1.994	0.5, 4.7	86.3/67.6
9a ³⁺	1.971 (1.959)	1.999 (1.973)	5.0, 10.4 (1.6, 1.6)	85.3/74.4, 93.5/65.0 (90.7/66.1, 90.7/66.1)
9b ³⁺	1.969 (1.963)	1.993 (1.973)	4.1, 5.8; ^e 3.9, 7.1 ^f (1.7, 1.7)	86.8/71.4, 92.5/67.9 ^e (89.7/65.8, 89.7/65.8); 95.9/68.4, ^f 92.2/72.0 ^g (89.7/65.8, 89.7/65.8), 149.9/154.7 ^h (165.3/119.4)
10a ³⁺	1.936	2.019	0.9, 45.1	44.8 ⁱ /63.8

^aThe values in parentheses refer to the energy-optimized structures determined by molecular mechanics calculations (Table 5). ^bFrom ref 7. ^cThis work, ref 8 reports 1.953 Å (M–N_{exo}), 2.007 Å (M–N_{endo}), and 2.7° (N_{endo}–C–C–N_{endo}) for 1b³⁺ and 1.952 Å (M–N_{exo}), 1.993 Å (M–N_{endo}), and 0.0° (N_{endo}–C–C–N_{endo}) for 2b³⁺ (see also ref 26). ^dprim–prim bridging. ^eCation 1. ^fCation 2. ^gMajor component of cation 2. ^hMinor component of cation 2. ⁱC–N_{exo}(Co)–C–O torsional angle.

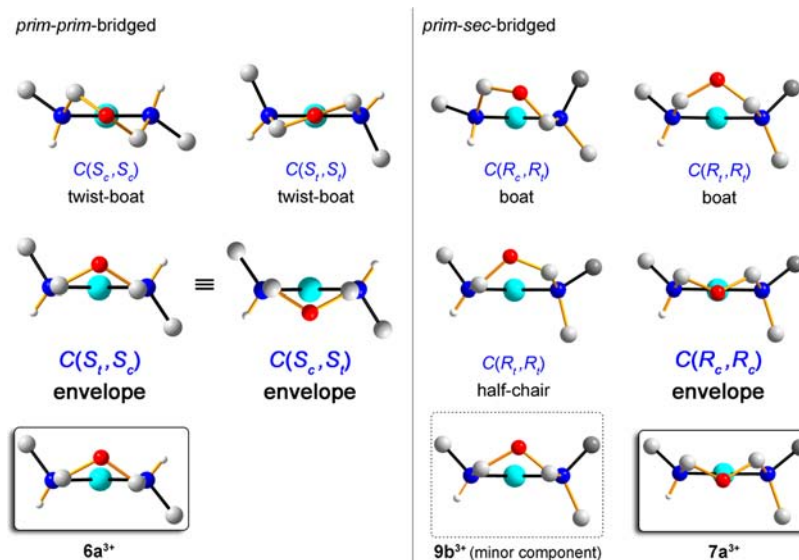


Figure 5. Different conformations of the six-membered Co–NRH–CH₂–O–CH₂–NRR' rings (see Table S2). The first and second row show the calculated conformations of the daza derivatives. The forms with lowest strain energy are highlighted. The third row (boxed structures) shows the conformations observed in the crystal structures. Color code: O, red; N, dark blue; Co, light blue (large); C, gray (the carbon atom of the ethylene residue of the daza frame is shown by darker gray); and H, small spheres. The bonds belonging to the torsional angle θ are highlighted in orange.³⁴

$$k_i = k_i^* \times [\text{OH}^-] \quad (6)$$

($i = 1, 2$) with pH-independent rate constants $k_1^*(\text{daza}) = 764 \pm 65$, $k_2^*(\text{daza}) = 9.5 \pm 2.8$, $k_1^*(\text{H}_2\text{O}, \text{Medaza}) = 1140 \pm 95$, $k_2^*(\text{H}_2\text{O}, \text{Medaza}) = 8.6 \pm 1.4$, $k_1^*(\text{D}_2\text{O}, \text{Medaza}) = 446 \pm 56$, and $k_2^*(\text{D}_2\text{O}, \text{Medaza}) = 3.4 \pm 1 \text{ s}^{-1} \text{ M}^{-1}$. Thus, the daza and Medaza derivatives show quite similar behavior.

The distinctly different rate constants k_1^* and k_2^* for the hydrolysis of singly and dibridged species 7³⁺ and 9³⁺ also opens a convenient route for the preparation of singly bridged derivatives

7³⁺. As can be seen in Table 2, the singly bridged species were, if at all, only obtained as a minor byproduct, whereas the dibridged 9³⁺ formed in high yields of up to 85%. For the synthesis of larger quantities of the singly bridged complexes, the detour via the dibridged product with subsequent controlled, partial hydrolysis is more efficient than a direct reaction.

DISCUSSION

Structure and Stability. It has frequently been observed that the bridging of two adjacent nitrogen donors in a Co^{III}

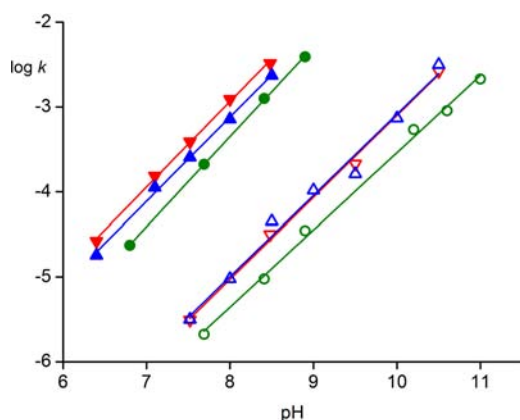


Figure 6. Dependence of the observed first-order rate constants k_1 and k_2 from pH (CV) or pH^* (NMR).¹² Closed symbols refer to experimental values for $9^{3+} \rightarrow 7^{3+}$ (k_1) and open symbols, for $7^{3+} \rightarrow 1^{3+}$ (k_2). The NMR experiments (D_2O) are shown in green³⁶ and the CV experiments for L in blue and for MeL in red color. The lines were calculated by linear regression analyses.

hexaamine complex by a three-atom strap increases steric strain either in the ligand sphere or in the ligand backbone.³⁷ The amount of additional strain strongly depends on the specific steric requirements of the complexes, and in many cases an enlargement of the hexaamine cavity is observed.^{4,37} Bridging of the two ligand moieties in 1^{3+} and 2^{3+} by oxidimethaneamine straps did indeed result in a slight shift of the $A_{1g}-T_{1g}$ transition to a longer wavelength (Table 4) as well as a moderate increase of the $\text{Co}^{\text{III}}/\text{Co}^{\text{II}}$ redox potential (110–130 mV per bridge). These observations, which can be interpreted in terms of a weakening of the ligand field and in a preference for accommodating the larger Co^{II} ion,³² are also reflected by the mean Co–N bond distances. The maximal value (1.989 Å) is indeed observed for dibridged 9a^{3+} , and the minimal value (1.966 Å), for nonbridged 1b^{3+} . As far as the mean bond distances are concerned, the effect is not, however, particularly pronounced. A slight increase of the mean Co–N bond distances coinciding with an increasing number of bridges could also be reproduced by the molecular mechanics study. On the basis of these calculations, the nonobservation of any trans-configured bridged species is due to increased nonbonding repulsion interactions (Table 5). A destabilization of the trans isomer was already observed to a minor extent for the parent daza and Medaza complexes.^{7,8} This effect is considerably enhanced in the bridged derivatives. It is thus quite obvious that the rearrangement from trans to cis, which is observed during the course of the bridging reaction, is driven by steric forces.

Because of the high rigidity of the $[\text{Co}(\text{daza})_2]$ scaffold, the most favorable conformation of the oxidimethaneamine bridges does not correspond to a chair form, as is usually observed for six membered chelate rings. In the C_2 -symmetric prim–prim-bridged structure, the calculations predict the lowest energy for a $C(S,S)$ diastereomer with an envelope conformation, where the Co, the two N, and the two C atoms all lie approximately in a plane (Figure 5). The oxygen atom is, however, significantly displaced and may flip between two positions below and above this plane. Two additional twist-boat forms are significantly more strained. In these two twist-boat forms, the H–N–H₂C–O torsional angle adopts either a cisoid (*c*) or transoid (*t*) orientation, with the cisoid form being in favor.³⁴ Moreover, the $C(S_p, S_t)$ structure obviously represents a shallow minimum. Already, some minor displacement prior to geometry opti-

mization forces a transformation into the more stable envelope form. Similarly, a chair conformation of the oxidimethaneamine bridges is disfavored for prim–sec-bridged structures. Less strained forms were located in a transient area of envelope/half chair/boat conformations (Figure 5). In general, the two forms with lowest energy again represent a flip of the oxygen atom combined with some minor movements of the methylene groups. In the singly bridged 7a^{3+} , the transoid form $C(R_p, R_t)$ is destabilized by an amount of 7.9 kJ/mol. Similarly, the cisoid–transoid conformer of doubly bridged 9a^{3+} is destabilized by 8.6 kJ/mol, and the strain energy of the bis-transoid conformer is increased by an additional 8.5 kJ/mol. For Medaza derivatives 7b^{3+} and 9b^{3+} , the calculated strain energies depended in a similar manner on the conformation of the NH–CH₂–O–CH₂–N bridges, with the increase in strain for a transoid conformation being slightly enlarged (10.2 kJ/mol for 7b^{3+} and 9.9 and 10.3 kJ/mol for 9b^{3+}). Adoption of cisoid low-strain forms have been confirmed in the crystal structures of 7a^{3+} , 7b^{3+} , and 9a^{3+} (Figure 1). In the dibridged Medaza derivative 9b^{3+} , one of the oxidimethaneamine bridges again adopted a cisoid conformation, whereas the other bridge is disordered with the cisoid and transoid form populating 74 and 26%, respectively (Figure S2).

A systematic discussion of diazepane ring conformation requires consideration of a total of 14 twist-chair (TC) and 14 chair (C) forms, which are generated by a series of consecutive pseudo-rotations.^{8,38,39} In the simple cycloheptane, the C_2 -symmetric TC and the C_s -symmetric C conformations are all equivalent in each case. For the 6-amino-1,4-diazepane derivative, however, the equivalency is partially lost, and a total of eight distinct C and of seven distinct TC forms (C1–C3, C6–C10, TC1, TC2, TC5–TC9 according to Espinosa's nomenclature, see Scheme S1) must be taken into account. Because of an unfavorable eclipsed arrangement within the ethylene subsets, the chair form is generally of some higher energy. The tridentate coordination mode requires such a chair (C3) with an axial primary amino group, and this conformation has indeed been observed in 1^{3+} , 2^{3+} , 3b^{3+} , 4b^{3+} , 6a^{3+} , 7^{3+} , 8b^{3+} , and 9^{3+} as well as for the tridentately coordinating daza subunit in 10a^{3+} (Table S3). Bridging interactions, involving one of the endocyclic nitrogen atoms as bridge head, appear, however, to induce some distortion, as indicated by a widening of the $\text{N}_{\text{endo}}-\text{C}-\text{N}_{\text{endo}}$ torsional angles up to a value of 10.4° (Table 6).⁴⁰ As recently discussed, the unfavorable chair conformation with its torsional strain facilitates the rupture of one of the M–N_{endo} bonds.⁸ The resulting bidentate coordination mode has a staggered conformation of the diamino-ethane moiety, resulting in a significant release of strain. Such a bidentate coordination mode still requires an axial orientation of the exocyclic amino group, as is provided by the forms TC1, TC2, TC5, or TC6. In 10a^{3+} the subunit with bidentate coordination adopted a TC2 conformation, whereas a TC5 conformation has been observed previously for the protonated HMedaza⁺ in $[\text{Cu}(\text{HMedaza})\text{Br}_3]$.⁸

Cleavage of Oxidimethaneamine Bridges. In a general approach, bridge cleavage may occur either by direct hydrolysis (k^h) or by an acid- (k^a) or base- (k^b) catalyzed mechanism, with an observed pH-dependent first-order rate constant $k^{\text{obs}} = k^a[\text{H}^+] + k^h + k^b K_w [\text{H}^+]^{-1}$. Possible catalysis by H^+ is, for instance, an initial protonation of an ether oxygen atom, and a possible base catalysis, an initial deprotonation of an H(–N–Co) bridge head (E1_{cb} mechanism). However, we have no indication for any direct hydrolysis of 7^{3+} and 9^{3+} by H_2O nor for an acid-catalyzed degradation. In fact, at room temperature acidic solutions of 9a^{3+} at pH 1 proved to be stable for a period of more than 7 years. In 6

M aqueous HCl, 7^{3+} and 9^{3+} are stable for several days even at an elevated temperature. We estimate the ratios $k^a/k^b < 10^{-11}$ and $k^h/k^b < 10^{-12}$. A sole base-catalyzed pathway is in line with the strictly linear dependence of $\log k^{\text{obs}}$ on pH in the range $6.4 \leq \text{pH} \leq 10.5$ (Figure 6). Therefore, assuming an E1_{cb} pathway,⁴¹ the initial H(-N-Co) deprotonation of a bridge-head is followed by a rupture of a C–O bond and a subsequent rapid hydrolysis of the resulting imine and aminol group. Above pH 10.5, we noted a slight flattening of the $\log k^{\text{obs}}$ versus pH curve. At first glance, such a behavior might be interpreted in terms of a saturation phenomenon in the E1_{cb} mechanism with the pH approaching the $\text{p}K_{\text{a}}$ of the relevant H(-N-Co) group.⁴² Deprotonation of amino groups coordinated to Co^{III} has frequently been discussed in the literature.^{43–46} In general, it is believed that a typical $\text{p}K_{\text{a}}$ for a hexamine-cobalt(III) complex lies around 15,^{43,44} but a significantly higher acidity has been accounted for some special cases.⁴⁵ However, as we will show in the next section, a corresponding deprotonation is expected to go along with an increased absorption around 400–600 nm,^{43,46} a behavior that has not been observed in our study. Investigation of the vis spectra in the course of the reaction ($6.4 \leq \text{pH} \leq 11.6$) shows only the expected properties for the Co^{III} -hexamine chromophores of 9^{3+} , 7^{3+} , and 1^{3+} . We therefore estimate the $\text{p}K_{\text{a}}$ of 7^{3+} or 9^{3+} to be >12.5 ,⁴⁷ and we explain the above-mentioned flattening of the $\log k^{\text{obs}}$ versus pH curve by experimental deficiencies as follows. The performance of a single NMR or CV experiment requires a total lead time of about 40 s (CV) or 2 min (NMR). Consequently, under conditions where the half live of the reaction approaches this value, the experimental requirements impede a precise measurement. At $\text{pH} \geq 11$, this is indeed the case.

Formation of Oxidimethaneamine Bridges. In contrast to the decomposition reaction, formation of 7^{3+} and 9^{3+} occurred in a heterogeneous mixture, and the interpretation of this process is not straightforward. In particular, it was not possible to conclude a mechanism by tracing the concentration of relevant species as a function of time. The only option was a careful analysis of the various products formed, which could be isolated under specific conditions (Table 2). A particularly striking observation was the dramatic influence of moisture on the reaction rate. We explain this effect by a catalytic action of water (or, more precisely, of the hydroxide ion) for the depolymerization of paraformaldehyde.⁴⁸ A further peculiar observation was the appearance of the above-mentioned strongly colored (almost black) product. A systematic variation of the addition of ingredients clearly established that all three components (the starting Co^{III} complex (1^{3+} or 2^{3+}), a base (NEt_3), and paraformaldehyde) are required for the formation of this particular product. Rapid filtration of the black, heterogeneous mixture in the absence of moisture allowed the isolation of a clear, dark-violet solution from which a vis spectrum could be recorded (Figure S1). The solution, which remained stable for some hours, exhibited two bands at 412 and 564 nm, with molar absorption coefficients in the range of about $400\text{--}500 \text{ M}^{-1} \text{ cm}^{-1}$. Such characteristics are indeed indicative of d–d transitions; however, in comparison with the starting material and with the finally formed bridged species 7^{3+} or 9^{3+} (Table 4), the bands adopted significant red shifts and increased intensities. All of these observations are compatible with a N–H deprotonation of a bridge head.^{43,46} Upon the addition of an excess of aqueous acid, an instantaneous color change from black to the usual yellowish-orange color, typical for a Co^{III} -hexamine complex, was noted. This is in agreement with a simple (diffusion controlled)

protonation reaction and supports the interpretation of the dark-colored species as deprotonation products of 7^{3+} and 9^{3+} . This hypothesis is further corroborated by the observation that yellowish-orange acetonitrile solutions of triflate salts of 7^{3+} and 9^{3+} immediately turned to a very dark, almost black, color upon NEt_3 -addition, with spectral properties being very similar to those observed in the formation process. Notably, the simple daza and Medaza complexes 1^{3+} and 2^{3+} and also the hemiaminal adduct 3b^{3+} do not show this type of reactivity. This again supports a selective deprotonation of the exocyclic amino group of the bridge head.⁴⁷ Curiously enough, a related strongly colored component was not detected in the reverse process (i.e., in the decomposition reaction of 7^{3+} and 9^{3+} in aqueous solution), although just such a deprotonation has been proposed as first step for the bridge degradation. However, as outlined above in the previous section, bridge degradation was performed in the range $6.4 < \text{pH} < 11.5$, whereas the $\text{p}K_{\text{a}}$ of the relevant exocyclic H(-N) bridge head in water has been estimated to a value of 13 to 14.⁴⁷ Therefore, the deprotonated species as a reactive intermediate would only form in minimal quantities below pH 11, and the nonobservance of strongly colored solutions in the degradation experiments as performed in this study would be well understandable. Such deprotonation products must, though, form at a $\text{pH} \geq 13$. Consequently, we performed experiments where small amounts of 7^{3+} or 9^{3+} dissolved in water were added to an excess of 1 M or 0.1 M KOH brine. Under these conditions, we could indeed observe instantaneous formation of a very short-lived, dark, almost black transient solution with a live time of less than one second.

The necessity for a trans \rightarrow cis rearrangement during the course of the bridging reaction is remarkable because low-spin Co^{III} is generally expected to be substitutionally inert. The rearrangement also disagrees with a previous study⁴ where *cis*- and *trans*- $[\text{Co}^{\text{III}}(\text{dapi})_2]^{3+}$ retained the orientation of the two dapi units in the bridging reaction, and distinctly distinguishable products were obtained for the two diastereomers. In this context, it is instructive to note that the chromatographic procedure applied to the reaction mixture often revealed some traces of Co^{2+} . This is understandable because formaldehyde can react as a reducing agent in the presence of a base. It appears likely that the observed trans \rightarrow cis isomerization occurs via a Co^{II} stage with subsequent reoxidation by aerial oxygen.

As outlined in the introduction, the attack of formaldehyde on a coordinated amino group primarily resulted in the formation of a corresponding carbinolamine. In the case of a primary amino group, a subsequent H_2O elimination and methylideneimine formation may occur. Interestingly, both types of the postulated intermediates could be isolated and characterized as byproducts in this investigation. A series of corresponding hemiaminals 3b^{3+} – 5b^{3+} has been obtained in the slow reaction of the trans complex 2b^{3+} (Table 2). Notably, these hemiaminals are the only species where the original trans orientation of the two diazepane frames was retained. We might thus regard them as early stages that are formed prior to the trans–cis-rearrangement step. Such hemiaminals are in general considered to be elusive and are usually not of sufficient stability to allow their isolation.^{30,49} In the crystal structure of 3b^{3+} and 4b^{3+} , the hydroxy-oxygen atoms are all hydrogen bonded to an (N-)H atom of an endocyclic amino group in the adverse ligand frame. Of the three possible bis-hemiaminals (C_{v} , C_{s} , and C_2), the C_2 -isomer did not form (Scheme 2). Because it is the only one where this type of hydrogen bonding would not be possible, the stabilization by such intramolecular $\text{HO}\cdots\text{H}-\text{N}_{\text{endo}}$ hydrogen bonding is

apparently a prerequisite for an isolation in the solid state. No hemiaminals have been obtained for *cis*-isomer **1b**³⁺ and for both daza analogs **1a**³⁺ and **2a**³⁺. For *cis*-isomer **1b**³⁺, a subsequent redox step is not required, and the subsequent condensation seemingly prevents an accumulation of a hemiaminal in the reaction mixture.

Is the reduction step $\text{Co}^{\text{III}} \rightarrow \text{Co}^{\text{II}}$ in general an imperative? The mechanism as outlined in the introduction (Scheme 1) does not require such a step. The observation that substantial amounts of free ligand are isolated in the reaction of **1**³⁺ or **2a**³⁺ together with the identification of some Co^{2+} in the final product indicates, however, that a considerable reduction does indeed occur for both isomers. Moreover, we could not observe significant differences in the overall reaction rate for *cis*-isomers **1**³⁺ and *trans*-isomers **2**³⁺. Because the reaction of *trans*-isomers **2**³⁺ must proceed via the Co^{II} stage, we can at least conclude that the reduction is either mandatory or it occurs at a rate comparable with the subsequent condensation process.⁵⁰

According to the general mechanism outlined in Scheme 1, the formation of an $\text{NH}-\text{CH}_2-\text{O}-\text{CH}_2-\text{N}$ bridge requires a synchronous formation of an imine and an aminol. For the formation of a *prim*-*sec*-bridged species, such as **7**³⁺ or **9**³⁺, this requirement is fulfilled without difficulties because the conversion of a primary and a secondary amine function into the corresponding imine and hemiaminal represents the end point of the condensation reaction in each case, respectively. This is different for the formation of a *prim*-*prim*-bridged species such as **6a**³⁺. The formation of such a species is not a priori implausible because the strain energy of the *prim*-*prim*-bridged **6a**³⁺ and the *prim*-*sec*-bridged **7a**³⁺ is quite similar (Table 5). However, for **6a**³⁺, bridge formation can only occur if one of the primary amino groups has been transformed completely into an imine, whereas the other one still remains at the hemiaminal stage.⁴ A complete condensation process of both primary amino groups would result in the formation of a diimine species such as **11b**³⁺. Clearly, the diimine represents a dead end and cannot proceed to the *prim*-*prim*-bridged product. Moreover, the competing attack of a hemiaminal originating from a secondary amino group would also impede formation of a *prim*-*prim*-bridged derivative. It is thus quite clear that formation of a complex such as **6a**³⁺ may be unlikely. It is remarkable that we could isolate it in a very small amount. However, as already mentioned in the Results section, we were not able to work out a reliable protocol for a reproducible preparation. We still do not understand which factors promote formation of a *prim*-*prim*-bridged species, and the isolation of **6a**³⁺ remains serendipitous. For a more in-depth analysis, one would require precise information about the reaction rate of hemiaminal formation for the primary as well as the secondary amino group and also for the subsequent transformation of the hemiaminal into an imine. In this regard, nothing at all is known to date. Similarly, we do not have any explicit evidence for how the rather exotic **10a**³⁺ could form. Both **6a**³⁺ and **10a**³⁺ are thus illustrative examples for the high complexity of the formation reaction. Molecular mechanics calculations evidently proved helpful for a qualitative location of major product components. However, the observation that the specific product distribution strongly depended on peripheral parameters (Table 2) and that a series of intermediates such as **8b**³⁺ has been isolated occasionally are strong indicators for a kinetic control of the reaction course. Product distribution thus relates on the energy of the transition states (ΔG^\ddagger) rather than the stability of the final products (ΔG). Although the two quantities are related (highly strained products already require

emergence of strain in the transition states), it is clear that a quantitative prediction of the product distribution is beyond the scope of such calculations. In contrast to the simple and straightforward analysis of the decomposition of **7**³⁺ and **9**³⁺, their formation must be regarded as the result of a multifaceted interplay of several partially competing processes, and a prediction of a precise product distribution still remains far from trivial.

CONCLUSIONS

In this investigation, we have corroborated that Co^{III} hexaamine complexes with ligands providing both primary and secondary amino groups readily react with paraformaldehyde, forming $\text{NH}-\text{CH}_2-\text{O}-\text{CH}_2-\text{N}$ bridges. The *cis*- and *trans*-isomers of $[\text{Co}(\text{daza})_2]^{3+}$ and $[\text{Co}(\text{Medaza})_2]^{3+}$ have been used as starting material. However, the bridged products always exhibit a *cis* configuration. On the basis of molecular mechanics calculation, we attribute this observation to increased steric strain within the molecular framework of the *trans* isomer. The rapid *cis*-*trans* isomerization that occurred during the course of reaction is unusual for Co^{III} and probably takes place at the Co^{II} stage. The bridges, which decay in an alkaline aqueous medium, reforming the original Co^{III} hexaamine complexes, are surprisingly stable in an acidic medium. The kinetics of the degradation process has been studied comprehensively. The only relevant pathway is a base-catalyzed reaction. We propose an initial $\text{H}(-\text{N}-\text{Co})$ deprotonation of the $\text{NH}-\text{CH}_2-\text{O}-\text{CH}_2-\text{N}$ bridges and a subsequent ring-opening followed by a rapid hydrolysis of the resulting imines and hemiaminals. Our investigation revealed that the daza and Medaza derivatives exhibited very similar reactivity. For both systems, the first bridge degrades at a considerably faster rate. We attribute the higher rate for the cleavage of the first bridge to the increased amount of steric strain in the dibridged species. The different rates cause accumulation of substantial portions of the singly bridged intermediates **7**³⁺ along the time course of the reaction, allowing preparative access to such species, even if they are not readily available by direct synthesis.

ASSOCIATED CONTENT

Supporting Information

Crystallographic data in CIF format; strain energies and puckering parameters; various conformations of the diazepane ring; vis spectrum of the dark colored product; molecular structures of **9b**³⁺, **1b**³⁺, and **2b**³⁺; C-H COSY NMR spectrum of **9a**³⁺; distribution of the torsional angle θ for bridged complexes. This material is available free of charge via the Internet at <http://pubs.acs.org>.

AUTHOR INFORMATION

Corresponding Author

*E-mail: hegetschweiler@mx.uni-saarland.de. Tel: (+49)-681-3022715. Fax: (+49)-681-3022663.

Notes

The authors declare no competing financial interest.

ACKNOWLEDGMENTS

Jens Burkhard and Eva Prinz performed some of the synthetic work. We thank Dr. Volker Huch (Universität des Saarlandes) for the collection of the X-ray diffraction data. Financial Support of the Deutsche Forschungsgemeinschaft (DFG Project HE 2799/3-2) is gratefully acknowledged.

REFERENCES

- (1) (a) Sargeson, A. M. *Pure Appl. Chem.* **1984**, *56*, 1603–1619. (b) Sargeson, A. M. *Pure Appl. Chem.* **1986**, *58*, 1511–1522. (c) Lawrance, G. A.; Maeder, M.; Wilkes, E. N. *Rev. Inorg. Chem.* **1993**, *13*, 199–232. (d) Bordunov, A. V.; Bradshaw, J. S.; Pastushok, V. N.; Izatt, R. M. *Synlett* **1996**, 933–948. (e) Nelson, J.; McKee, V.; Morgan, G. *Prog. Inorg. Chem.* **1998**, *47*, 167–316. (f) Costisor, O.; Linert, W. *Rev. Inorg. Chem.* **2000**, *20*, 63–127.
- (2) Höhn, A.; Geue, R. J.; Sargeson, A. M.; Willis, A. C. *J. Chem. Soc., Chem. Commun.* **1989**, 1648–1649.
- (3) (a) Larsen, E.; Larsen, S.; Lunding, G. *Inorg. Chem.* **1988**, *27*, 3051–3054. (b) Hegetschweiler, K.; Weber, M.; Huch, V.; Geue, R. J.; Rae, A. D.; Willis, A. C.; Sargeson, A. M. *Inorg. Chem.* **1998**, *37*, 6136–6146. (c) Bernhardt, P. V.; Jones, L. A. *J. Chem. Soc., Dalton Trans.* **1998**, 1757–1761.
- (4) Pauly, J. W.; Sander, J.; Kuppert, D.; Winter, M.; Reiss, G. J.; Zürcher, F.; Hoffmann, R.; Fässler, T. F.; Hegetschweiler, K. *Chem.—Eur. J.* **2000**, *6*, 2830–2846.
- (5) Geue, R. J.; Snow, M. R.; Springborg, J.; Herlt, A. J.; Sargeson, A. M.; Taylor, D. *J. Chem. Soc., Chem. Commun.* **1976**, 285–287.
- (6) Brothers, P. J.; Clark, G. R.; Palmer, H. R.; Ware, D. C. *Inorg. Chem.* **1997**, *36*, 5470–5477.
- (7) Romba, J.; Kuppert, D.; Morgenstern, B.; Neis, C.; Steinhauser, S.; Weyhermüller, T.; Hegetschweiler, K. *Eur. J. Inorg. Chem.* **2006**, 314–328.
- (8) Neis, C.; Petry, D.; Demangeon, A.; Morgenstern, B.; Kuppert, D.; Huppert, J.; Stucky, S.; Hegetschweiler, K. *Inorg. Chem.* **2010**, *49*, 10092–10107.
- (9) (a) Aime, S.; Calabi, L.; Cavallotti, C.; Gianolio, E.; Giovenzana, G. B.; Losi, P.; Maiocchi, A.; Palmisano, G.; Sisti, M. *Inorg. Chem.* **2004**, *43*, 7588–7590. (b) Peralta, R. A.; Neves, A.; Bortoluzzi, A. J.; Casellato, A.; dos Anjos, A.; Greatti, A.; Xavier, F. R.; Szpoganicz, B. *Inorg. Chem.* **2005**, *44*, 7690–7692. (c) Bortoluzzi, A. J.; Neves, A.; Terra, G. G. *Acta Crystallogr., Sect. E* **2006**, *62*, 2965–2966.
- (10) In the numbering scheme used in this Article, **a** refers to daza and **b** to corresponding Medaza derivatives. The absence of this sublabel indicates consideration of both complexes. As an example, *cis*-[Co(daza)₂]³⁺ is abbreviated with **1a**³⁺ and *cis*-[Co(Medaza)₂]³⁺ with **1b**³⁺. The label **1**³⁺ thus refers to **1a**³⁺ and **1b**³⁺.
- (11) (a) Hurd, R. E. *J. Magn. Reson.* **1990**, *87*, 422–428. (b) von Kienlin, M.; Moonen, C. T. W.; van der Toorn, A.; van Zijl, P. C. M. *J. Magn. Reson.* **1991**, *93*, 423–429. (c) Hurd, R. E.; John, B. K. *J. Magn. Reson.* **1991**, *91*, 648–653. (d) Ruiz-Cabello, J.; Vuister, G. W.; Moonen, C. T. W.; van Gelderen, P.; Cohen, J. S.; van Zijl, P. C. M. *J. Magn. Reson.* **1992**, *100*, 282–302. (e) Willker, W.; Leibfritz, D.; Kerssebaum, R.; Bermel, W. *Magn. Reson. Chem.* **1993**, *31*, 287–292.
- (12) In this Article, the term pH* refers to the direct pH meter reading (Metrohm 713 pH meter) of the D₂O samples using a Metrohm glass electrode with an aqueous (H₂O) Ag/AgCl reference that was calibrated with aqueous (H₂O) buffer solutions. For the interconversion of pH* and pD see: Alderighi, L.; Bianchi, A.; Biondi, L.; Calabi, L.; De Miranda, M.; Gans, P.; Ghelli, S.; Losi, P.; Paleari, L.; Sabatini, A.; Vacca, A. *J. Chem. Soc., Perkin Trans. 2* **1999**, 2741–2745.
- (13) *CRC Handbook of Chemistry and Physics*, 90th ed.; Lide, D. R., Ed.; CRC Press: Boca Raton, FL, 2009–2010.
- (14) Bartholomä, M.; Gisbrecht, S.; Stucky, S.; Neis, C.; Morgenstern, B.; Hegetschweiler, K. *Chem.—Eur. J.* **2010**, *16*, 3326–3340.
- (15) *HyperChem*, release 7.51 for Windows; Hypercube Inc.: Gainsville, FL, 2002.
- (16) (a) Comba, P.; Hambley, T. W.; Lauer, G.; Okon, N. *MOMECS97, a Molecular Modeling Package for Inorganic Compounds*; University of Heidelberg: Heidelberg, Germany, 1997. (b) Bol, J. E.; Buning, C.; Comba, P.; Reedijk, J.; Ströhle, M. *J. Comput. Chem.* **1998**, *19*, 512–523. (c) Comba, P.; Hambley, T. W. *Molecular Modeling of Inorganic Compounds*; VCH: Weinheim, Germany, 1995.
- (17) Kuppert, D.; Comba, P.; Hegetschweiler, K. *Eur. J. Inorg. Chem.* **2006**, 2792–2807.
- (18) Bygott, A. M. T.; Sargeson, A. M. *Inorg. Chem.* **1998**, *37*, 4795–4806.
- (19) Comba, P.; Maeder, M.; Zipper, L. *Helv. Chim. Acta* **1989**, *72*, 1029–1037.
- (20) Dixon, N. E.; Lawrance, G. A.; Lay, P. A.; Sargeson, A. M.; Taube, H. *Inorg. Synth.* **1986**, *24*, 243–306.
- (21) A careful washing of the trifluoromethanesulfonate salts **1a**(CF₃SO₃)₃, **2a**(CF₃SO₃)₃, **1b**(CF₃SO₃)₃, and **2b**(CF₃SO₃)₃ with Et₂O is required to remove traces of triflic acid. In addition, the trifluoromethanesulfonate salts are highly hygroscopic.
- (22) Sheldrick, G. M. *Acta Crystallogr., Sect. A* **2008**, *64*, 112–122.
- (23) Cremer, D.; Pople, J. A. *J. Am. Chem. Soc.* **1975**, *97*, 1354–1358.
- (24) Spek, A. L. *PLATON, A Multipurpose Crystallographic Tool*; Utrecht University: Utrecht, The Netherlands, 2011; see also: Spek, A. L. *Acta Crystallogr., Sect. D* **2009**, *65*, 148–155.
- (25) Flack, H. D. *Acta Crystallogr., Sect. A* **1983**, *39*, 876–881.
- (26) The crystal structures of **1b**(ClO₄)₃·H₂O and **2b**Br₃·H₂O have already been reported.⁸ However, some disorder was noted for one of the perchlorate anions. We changed the counterions and now report results with improved accuracy for both complexes. Graphical representations of their molecular structures are given in the Supporting Information (Figure S3).
- (27) NMR data of **11b**³⁺. Methyl groups: 1.58 ppm (s, 6H). Methylideneimino groups: 7.91 ppm (d, *J* = 5 Hz, 2H); 7.69 (d, *J* = 5 Hz, 2H).
- (28) In this context, the expression “reaction rate” exclusively refers to purely phenomenological observations and not to any rate law.
- (29) (a) Gainsford, G. J.; Geue, R. J.; Sargeson, A. M. *J. Chem. Soc., Chem. Commun.* **1982**, 233–235. (b) Geue, R. J.; McCarthy, M. G.; Sargeson, A. M.; Skelton, B. W.; White, A. H. *Inorg. Chem.* **1985**, *24*, 1607–1609.
- (30) Ng, C.-H.; Teo, S.-B.; Teoh, S.-G.; Fun, H.-K.; Declercq, J.-P. *Inorg. Chim. Acta* **2002**, *340*, 81–86.
- (31) Signals of the H(-N) hydrogen atoms of **7**³⁺ and **9**³⁺ could be observed in the range of 6–8 ppm. However, the H versus D exchange was found to be rapid even in an acidic medium. As an example, the H(-N) signals of **9a**³⁺ at 6.93 and 7.99 ppm disappeared completely within 15 min in a 0.05 M DCl/D₂O solution at ambient temperature.
- (32) Brown, K. N.; Geue, R. J.; Hambley, T. W.; Hockless, D. C. R.; Rae, A. D.; Sargeson, A. M. *Org. Biomol. Chem.* **2003**, *1*, 1598–1608.
- (33) Connelly, N. G.; Damhus, T.; Hartshorn, R. M.; Hutton, A. T. *Nomenclature of Inorganic Chemistry. IUPAC Recommendations 2005*; RSC Publishing: Cambridge, United Kingdom, 2005.
- (34) In the various structures under consideration, the H–N_{exo}–C–O or C_{propylene}–N_{endo}–C–O torsional angle θ clusters around 30–95° (cisoid = *c*) or 114–180° (transoid = *t*), see Figure S5. The usual classification synperiplanar (0° < θ < 30°), synclinal (30° < θ < 90°), anticlinal (90° < θ < 150°), and antiperiplanar (150° < θ < 180°) is not expedient in this particular case. In a given (X_a, Y_b) pair (X, Y = R, S; a, b = *c*, *t*), the first label refers to the configuration of N_{exo}.
- (35) Dibridged **9b**³⁺ and the final, nonbridged **1b**³⁺ adopt C₂ symmetry and display one signal for the two homotopic methyl groups at 1.33 and 1.38 ppm, respectively, whereas the singly bridged, C₁-symmetric intermediate **7b**³⁺ exhibits two signals for the diastereotopic methyl groups at 1.32 and 1.43 ppm.
- (36) As can be seen in Figure 6, the reaction in D₂O was generally found to be slightly slower ($k^{\text{H}_2\text{O}}/k^{\text{D}_2\text{O}} \approx 2.5$). We attribute this phenomenon to the lower temperature (CV, 25 °C; NMR, 21 °C) and to the well-known D versus H isotope effect.
- (37) (a) Comba, P.; Sickmüller, A. F. *Angew. Chem., Int. Ed. Engl.* **1997**, *36*, 2006–2008. (b) Comba, P. *Coord. Chem. Rev.* **1999**, *182*, 343–371.
- (38) (a) Espinosa, A.; Gallo, M. A.; Entrena, A.; Gomez, J. A. *J. Mol. Struct.* **1994**, *326*, 249–260. (b) Entrena, A.; Campos, J.; Gomez, J. A.; Gallo, M. A.; Espinosa, A. *J. Org. Chem.* **1997**, *62*, 337–349. (c) Entrena, A.; Campos, J. M.; Gallo, M. A.; Espinosa, A. *ARKIVOC* **2005**, 88–108.
- (39) Parker, D.; Waldron, B. P. *Org. Biomol. Chem.* **2013**, *11*, 2827–2838.
- (40) Parker, D.; Waldron, B. P.; Yufit, D. S. *Dalton Trans.* **2013**, *42*, 8001–8008.

(41) The observation that the H(-N) hydrogen atoms of the bridge heads are readily exchanged in D₂O,³¹ and the moderate kinetic isotope effect³⁶ are in line with an E1_{cb} mechanism.

(42) Sargeson, A. M. *Pure Appl. Chem.* **1973**, *33*, 527–544.

(43) Goodall, D. M.; Hardy, M. J. *J. Chem. Soc., Chem. Commun.* **1975**, 919–921.

(44) Wilinski, J.; Kurland, R. J. *Inorg. Chem.* **1973**, *12*, 2202–2203.

(45) Comba, P.; Sargeson, A. M. *J. Chem. Soc., Chem. Commun.* **1985**, 51–52.

(46) Geue, R. J.; Hambley, T. W.; Harrowfield, J. M.; Sargeson, A. M.; Snow, M. R. *J. Am. Chem. Soc.* **1984**, *106*, 5478–5488.

(47) Because of the electron-withdrawing effect of the ether oxygen atom, the pK_a of the Co–HNR–CH₂–O moieties in 7³⁺ or 9³⁺ is expected to be decreased. An analogous situation is known for aliphatic alcohols such as MeOH or EtOH, which have a similar pK_a to that of normal hexaamine-cobalt(III)-complexes. The incorporation of an additional geminal oxygen atom, as featured in the hydrates of formaldehyde or acetaldehyde, lowers the pK_a to 13 to 14 (see: Bell, R. P.; McTigue, P. T. *J. Chem. Soc.* **1960**, 2983–2994) and a similar value could thus also be expected for 7³⁺ and 9³⁺.

(48) Löbering, J. *Ber. Dtsch. Chem. Ges.* **1936**, *69*, 1844–1854.

(49) Iwasawa, T.; Hooley, R. J.; Rebek, J., Jr. *Science* **2007**, *317*, 493–496.

(50) One may argue that we did not isolate any free ligand in the slow reaction with the Medaza complex 2b³⁺ (Table 2). However, it must be kept in mind that the chromatographic procedure allowed only the isolation of colored fractions, and the colorless free ligand was in each case isolated only coincidentally because it moved together with the singly bridged 7³⁺. In cases where no singly bridged species were isolated, such as the slow reaction of 2b³⁺, the free ligand was not isolated even if it would have formed.